AFRL-AFOSR-UK-TR-2022-0005

Determination of the Length Scale Parameter in Peridynamics

Oterkus, Erkan
UNIVERSITY OF STRATHCLYDE VIZ ROYAL COLLEGE OF SCIENCE & TECHNOLOGY
16 RICHMOND STREET
50 RICHMOND ST
GLASGOW, LANARKSHIRE, G1 1XT
GBR

11/19/2021
Final Technical Report

Air Force Research Laboratory
Air Force Office of Scientific Research
European Office of Aerospace Research and Development
Unit 4515 Box 14, APO AE 09421

REPORT DOCUMENTATION PAGE

Form Approved
OMB No. 0704-0188

1. REPORT DATE *(DD-MM-YYYY)*	**2. REPORT TYPE**	**3. DATES COVERED** *(From - To)*
19-11-2021	Final	20 Aug 2018 - 19 Aug 2021

4. TITLE AND SUBTITLE
Determination of the Length Scale Parameter in Peridynamics

5a. CONTRACT NUMBER

5b. GRANT NUMBER
FA9550-18-1-7004

5c. PROGRAM ELEMENT NUMBER
61102F

6. AUTHOR(S)
Erkan Oterkus

5d. PROJECT NUMBER

5e. TASK NUMBER

5f. WORK UNIT NUMBER

7. PERFORMING ORGANIZATION NAME(S) AND ADDRESS(ES)
UNIVERSITY OF STRATHCLYDE VIZ ROYAL COLLEGE OF SCIENCE & TECHNOLOGY
16 RICHMOND STREET
50 RICHMOND ST
GLASGOW, LANARKSHIRE G1 1XT
GBR

8. PERFORMING ORGANIZATION REPORT NUMBER

9. SPONSORING/MONITORING AGENCY NAME(S) AND ADDRESS(ES)
EOARD
UNIT 4515
APO AE 09421-4515

10. SPONSOR/MONITOR'S ACRONYM(S)
AFRL/AFOSR IOE

11. SPONSOR/MONITOR'S REPORT NUMBER(S)
AFRL-AFOSR-UK-TR-2022-0005

12. DISTRIBUTION/AVAILABILITY STATEMENT
A Distribution Unlimited: PB Public Release

13. SUPPLEMENTARY NOTES

14. ABSTRACT
Peridynamics is based on integro-differential equations and does not contain any spatial derivatives which makes it suitable for predicting failure initiation and propagation. It also has a length scale parameter called horizon, which gives peridynamics a non-local character. This research expanded the body of knowledge of research on Peridynamics by determining optimum horizon sizing for bond-based peridynamics, ordinary state-based peridynamics and non-ordinary state-based peridynamics. It introduces the use of a dual-horizon peridynamic framework for non-uniform discretization and variable horizon sizes and investigates aspects of non-local behavior. Further, this research extends Dual Horizon Peridynamics formulation to thermal diffusion analysis. Finally, the research introduced methods to handle cases with damage and reduce the computation time required to conduct peridynamic simulations. This research resulted in five peer reviewed journal with an additional four articles submitted for publication. This research was presented at nine technical conferences

15. SUBJECT TERMS

16. SECURITY CLASSIFICATION OF:			**17. LIMITATION OF ABSTRACT**	**18. NUMBER OF PAGES**	**19a. NAME OF RESPONSIBLE PERSON**
a. REPORT	**b. ABSTRACT**	**c. THIS PAGE**			MARK FRIEND
U	U	U	SAR	43	**19b. TELEPHONE NUMBER** *(Include area code)* 314-235-6292

Final Report for EOARD Grant FA9550-18-1-7004

"**Determination of the Length Scale Parameter in Peridynamics**"

11/17/2021

Name of Principal Investigators (PI and Co-PIs): Dr. Erkan Oterkus (PI),Dr. Selda Oterkus (Co-PI)
- e-mail address : erkan.oterkus@strath.ac.uk
- Institution : University of Strathclyde
- Mailing Address : 100 Montrose Street Glasgow G4 0LZ United Kingdom
- Phone : +44-141-548-3876
- Fax :

Period of Performance: 08/20/2018 – 08/19/2021

Abstract:

Peridynamics is a new continuum mechanics formulation and has several advantages with respect to classical continuum mechanics formulation which is widely used in structural analysis. Peridynamics is based on integro-differential equations and does not contain any spatial derivatives which makes it suitable for predicting failure initiation and propagation. It also has a length scale parameter called horizon which gives peridynamics a non-local character. Numerical implementation of peridynamics is usually done by using meshless method. Therefore, the solution domain is discretised into volumes represented by a material point at its center. Due to the non-local nature of peridynamics, material points are interacting with each other even if they are far apart. The interaction range is defined by the horizon size and shape. The horizon size should be chosen depending on the nature of the problem.

First, we focus on problems showing classical deformation behaviour. Therefore, the selected horizon size should allow the peridynamic solution to capture the same behaviour as the classical solution. Currently, there are three main peridynamic formulations available in the literature including bond-based peridynamics, ordinary state-based peridynamics and non-ordinary state-based peridynamics. In this study, the optimum horizon size is determined for all these three formulations by using uniform discretisation and under dynamic and static conditions. Application of boundary conditions is different in peridynamics with respect to classical continuum mechanics formulation. An elegant approach is presented for representing displacement constraints and traction boundary conditions using a fictitious region approach.

In practical applications, it is not always suitable to use uniform discretisation in all parts of the solution domain. Instead, non-uniform discretisation can be utilised. In peridynamics such formulation can introduce numerical error if variable horizon sizes are used at different parts of the domain since it can cause lack of interactions at the interfaces. In this study, a new formulation is presented in dual-horizon peridynamic framework for non-uniform discretisation and variable horizon sizes. It is shown that the horizon sizes selected as optimum sizes for uniform discretisation can also be used for non-uniform discretisation without introducing significant error to the system.

The effect of the shape of the horizon is also investigated. It is concluded that the square shape

horizon is not suitable for bond-based and ordinary-state based peridynamics. On the other hand, non-ordinary state-based peridynamics is not sensitive to the shape of the horizon.

Next, we investigate aspects of peridynamics related to non-local material behaviour without considering damage. A new multi-horizon formulation is introduced. The new formulation has a potential of both improving accuracy and capturing non-local effects. In addition, the horizon size is determined for various materials by using dispersion relationships and compared against experimental data and lattice dynamics model. Analytical expressions of dispersion relationships from peridynamic theory are also provided. Moreover, application of peridynamics to surface elasticity is demonstrated which is especially important for modelling structures at nano-scale.

Dual Horizon Peridynamics formulation is also extended for thermal diffusion analysis. Lagrangian formalism is utilised to derive the governing equations. The proposed formulation allows utilisation of variable discretisation and horizon sizes inside the solution domain which can result in significant benefits in terms of computational time. To demonstrate the capability of the Dual Horizon Peridynamics formulation, three different example problems are considered including a square plate with temperature and no flux boundary conditions, a square plate under thermal shock loading, and a square plate with an insulated crack. For all problems that are considered good agreement is obtained between peridynamics (PD) predictions and finite element method (FEM) results.

For the cases with damage, horizon size is determined by comparing peridynamic results with nonlocal elasticity solution. Moreover, horizon size is also determined by considering the plasticity field around the crack tip. In addition, a computational homogenization framework is presented for non-ordinary state-based peridynamics. Finally, to reduce the computational time of peridynamic simulations, static condensation of the peridynamic heat conduction model is introduced.

Keywords: peridynamics; non-local; horizon; crack

Introduction:

Peridynamics [1] is a non-local continuum mechanics formulation and it has a length scale parameter called horizon. Determination of the size of the length scale parameter is an essential step to obtain accurate results from peridynamic simulations. In this project, we both determine the horizon sizes for both ordinary-state based peridynamics formulation and non-ordinary state based formulations [2]. Different conditions exist in practice and each condition requires a different approach to determine the length scale parameter. In this project, these conditions are split into three different categories, so that we can eliminate the simultaneous influence of different effects on each other. Hence, the primary objective of this study is to determine the length scale parameter for the following conditions:

1. Classical deformation behavior in problems without damage: We start with a condition that there is no existence of damage in the structure and non-local effects are insignificant. For such a condition, peridynamic solution should converge to the classical continuum mechanics solution as horizon size converges to 0 [2]. Therefore, in this case, classical continuum mechanics solution can serve as a reference solution for peridynamics. Comparing peridynamic results against analytical and finite

element method solutions is sufficient to make decisions on the suitable value of horizon size.

Several important aspects are explored:

- For uniform discretization, what should be the size of the horizon with respect to the grid spacing and the size of the solution domain?
- For non-uniform discretization, what should be the horizon size that we can use at different parts of the solution domain?
- For the shape of the horizon, it is a general trend to choose a spherical domain for 3-Dimensional problems and a circular domain for 2-Dimensional problems. What happens if a different shape is chosen?

2. Non-classical (non-local) deformation behavior in problems without damage: In the second task, we look into problems inheriting non-local characteristics without considering damage. Note that as opposed to the Task 1 where horizon being considered as a numerical parameter, in this task, it corresponds to a physical parameter which requires a careful selection of this parameter to capture the actual physics of the problem.

In this task, we investigate several important aspects:

- How many length scale parameters that we will need to describe non-local behavior?
- How can we determine horizon size by comparing against dispersion relationships obtained from experiments and lattice models?
- In nano-materials, material properties close to the surfaces can be different than bulk properties. This variation causes surface stresses. How can we incorporate surface elasticity models in peridynamic framework?

3. Non-locality in problems with damage: In the third task, we look into problems with damage. The occurrence of damage introduces a new length scale to the problem especially around the damage region. Therefore, it is essential to determine the value of this length scale parameter and relate it to the horizon size. It is also important to investigate if the length scale parameter changes as the damage size changes. We compare peridynamics with non-local elasticity to determine the horizon size suitable to represent the non-local behavior around the damage region.

Linear Elastic Fracture Mechanics (LEFM) assumes sharp crack tip and the formulation ignores process zone which leads to unphysical stresses at the crack tips. The infinite stresses can disappear by considering the process zone at the crack tip regions as demonstrated by Dugdale [3]. Peridynamics can also yield non-singular stresses at the crack tip and can capture the process zone at the crack tip (see Fig. 1).

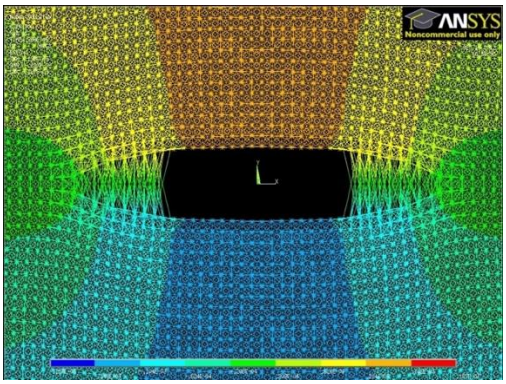

Figure 1. Peridynamic prediction of process zone at the crack tips.

In this part of the project, based on the peridynamic plasticity model developed by Madenci and Oterkus [4], horizon size is determined to capture accurate plasticity behavior around the crack tip region.

For each of the three tasks described earlier, necessary mathematical proofs are provided in a way that such proofs can also be easily adapted by engineering community. Moreover, the mathematical proofs are supported by numerical solutions and these solutions are compared against analytical, numerical and experimental data corresponding to benchmark cases which are produced during the project or available data from the literature are utilized.

Experiment:

This section provides detailed information about the methods, assumptions and procedures for bond-based peridynamics, state-based peridynamics, dual-horizon peridynamic formulation, multi-horizon peridynamic formulation, peridynamic dispersion relationships and determination of horizon size with/without considering the effect of damage and nonlocal effects, surface elasticity, computational homogenization framework for non-ordinary state-based peridynamics and static condensation of the peridynamic heat conduction model.

Peridynamic theory

Bond-based peridynamics

Peridynamics (PD) was introduced by Silling [1] as a new continuum mechanics formulation. As opposed to Cauchy's classical continuum mechanics (CCM) formulation, Silling relaxed the condition of interaction of material points which are directly in contact with each other. Instead, all material points inside the structure can interact with each other. In peridynamics, an influence domain is defined to limit the range of interactions which is called horizon, $H_{\mathbf{x}}$ (Fig. 2). Moreover, the equation of motion doesn't contain any spatial derivatives. Therefore, these equations are always valid regardless of discontinuities. The equation of motion of peridynamics can be expressed as

$$\rho(\mathbf{x})\ddot{\mathbf{u}}(\mathbf{x},t) = \int_{H_{\mathbf{x}}} \mathbf{f}\left(\mathbf{u}'-\mathbf{u},\mathbf{x}'-\mathbf{x}\right)dV' + \mathbf{b}(\mathbf{x},t) \tag{1}$$

where $\mathbf{f}\left(\mathbf{u}'-\mathbf{u},\mathbf{x}'-\mathbf{x}\right)$ represents the interaction (bond) force between material points $\mathbf{x}$ and $\mathbf{x}'$ and $\mathbf{u}$ is the displacement of the material point $\mathbf{x}$.

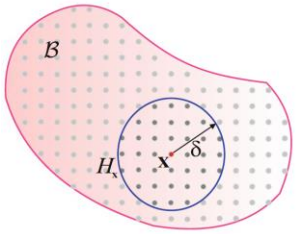

Figure 2. Peridynamics and horizon concept

The definition of the interaction force depends on the material behaviour. For linear elastic isotropic materials, it can be considered as a spring force. However, it is represented in a slightly different form as

$$\mathbf{f}\left(\mathbf{u}'-\mathbf{u},\mathbf{x}'-\mathbf{x}\right)=c\,s\,\frac{\mathbf{y}'-\mathbf{y}}{\left|\mathbf{y}'-\mathbf{y}\right|} \tag{2}$$

where $\mathbf{y}=\mathbf{x}+\mathbf{u}$ is the position of the material point $\mathbf{x}$ in the deformed configuration. In Eq. (2), c denotes bond constant and s is the stretch of the bond which can be defined as

$$s=\frac{\left|\mathbf{y}'-\mathbf{y}\right|-\left|\mathbf{x}'-\mathbf{x}\right|}{\left|\mathbf{x}'-\mathbf{x}\right|} \quad . \tag{3}$$

The interaction force is calculated in the deformed configuration. In the original peridynamic formulation (bond-based peridynamics), it is assumed that the force between two points are equal and opposite to each other (Fig. 3). Bond constant is the material parameter of peridynamics and can be expressed in terms of material constants of CCM. These relationships can be established by considering a common parameter used in both approaches. For instance, strain energy density of a material point can be used for this purpose. An imaginary structure can be considered and this structure can be subjected to a simple loading condition. A material point inside this structure should be identified and its strain energy density can be calculated by using both peridynamics and CCM. Since the value of strain energy density calculated from both approaches should be the same, a relationship between peridynamics parameters and material constants of CCM can be established. For a linear elastic isotropic material, this relationship can be expressed for 3-Dimensional models as

$$c=\frac{12E}{\pi\,\delta^4} \tag{4}$$

where δ is the size of the horizon. Note that there is only one peridynamic parameter used in the bond-based peridynamics formulation as opposed to two independent material parameters of CCM which can be chosen as elastic modulus, E and Poisson's ratio, ν. Because of this mismatch, one of the parameters of CCM is constant. In other words, it is not possible to freely define Poisson's ratio value since peridynamic formulation automatically captures a constant Poisson's ratio value which is $1/4$ for 3-Dimensional models. For materials which have Poisson's ratio value different than this value, advanced versions of peridynamic formulations should be used. Currently the most common

advanced peridynamic approaches are ordinary state-based peridynamics and non-ordinary state-based peridynamics.

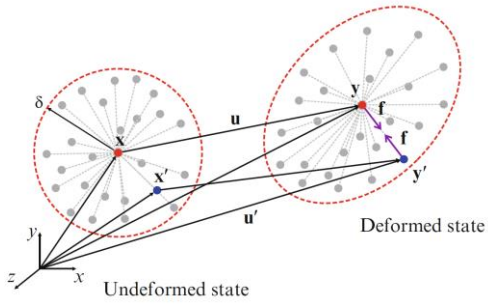

Figure 3. Bond-based peridynamics

Ordinary state-based peridynamics

As mentioned earlier, the original bond-based peridynamic formulation encounters a limitation on material constants since it was assumed that the peridynamic force between two material points are equal and opposite to each other. Moreover, the peridynamic force between two material points only depends on the motion of associated material points. In order to eliminate the limitation of bond-based peridynamic formulation, its assumptions should be relaxed. In other words, it can be assumed that the magnitude of the force between two materials do not have to be equal to each other (Fig. 4). In addition to this, this force can depend on not only the motion of associated material points, but also the motion of their family members. Based on these new assumptions, the equation of motion of a material point can be written as

$$\rho(\mathbf{x})\ddot{\mathbf{u}}(\mathbf{x},t)=\int_{H_{\mathbf{x}}}\left\{\underline{\mathbf{T}}(\mathbf{x},t)\langle\mathbf{x}'-\mathbf{x}\rangle-\underline{\mathbf{T}}(\mathbf{x}',t)\langle\mathbf{x}-\mathbf{x}'\rangle\right\}dV'+\mathbf{b}(\mathbf{x},t) \tag{5}$$

or

$$\rho(\mathbf{x})\ddot{\mathbf{u}}(\mathbf{x},t)=\int_{H_{\mathbf{x}}}(\mathbf{t}-\mathbf{t}')\,dV'+\mathbf{b}(\mathbf{x},t) \tag{6}$$

where $\underline{\mathbf{T}}\langle\bullet\rangle$ represents the force state which is a new terminology in state-based peridynamics [2] and $\mathbf{t}$ is the peridynamic force that material point $\mathbf{x}'$ is exerting on $\mathbf{x}$.

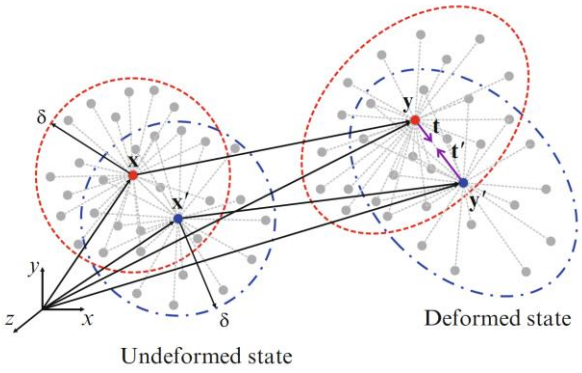

Figure 4. Ordinary state-based peridynamics

State is basically an infinite dimensional array or matrix and stores information about a particular parameter of peridynamic bonds associated with a particular material point. Therefore, force state stores the peridynamic forces belonging to peridynamic bonds. When the state operates on a particular bond, it only returns the stored value for that particular bond. For a linear elastic isotropic material, the force state can be expressed as

$$\underline{\mathbf{T}}\left(\mathbf{x},t\right)\left\langle \mathbf{x}'-\mathbf{x}\right\rangle =\mathbf{t}=\left(\frac{2ad\delta}{\left|\mathbf{x}'-\mathbf{x}\right|}\theta\left(\mathbf{x},t\right)+b\,s\right)\frac{\mathbf{y}'-\mathbf{y}}{\left|\mathbf{y}'-\mathbf{y}\right|} \tag{7}$$

where a, b and d are peridynamic parameters and $\theta\left(\mathbf{x},t\right)$ is peridynamic dilatation term which can be defined as

$$\theta\left(\mathbf{x},t\right)=\int_{H_{\mathbf{x}}}\left(d\,\delta s\right)dV' \tag{8}$$

Non-ordinary state-based peridynamics

As mentioned earlier, in ordinary-state based peridynamics formulation, although the peridynamic forces between two material points can have different magnitudes, their directions are assumed to be along the bond direction. This assumption can be disregarded by allowing the direction of peridynamic forces in arbitrary directions (Fig. 5). By doing this, it is essential to explicitly impose a condition on conservation of angular momentum since it is not automatically conserved as in bond-based and ordinary-state based formulations. Therefore, the following relationship must hold:

$$\int_{H_{\mathbf{x}}}\left\{\left(\mathbf{y}'-\mathbf{y}\right)\times\underline{\mathbf{T}}\left(\mathbf{x},t\right)\left\langle \mathbf{x}'-\mathbf{x}\right\rangle\right\}dV'=0 \tag{9}$$

Moreover, the peridynamic force between two material points can be expressed in terms of appropriate stress definitions of CCM. Such an approach can allow direct integration of material models in CCM into peridynamics. For instance, a peridynamic force can be related to the first Piola-Kirchhoff (Lagrangian) stress tensor, $\mathbf{P}$ as

$$\underline{\mathbf{T}}\left(\mathbf{x},t\right)\left\langle \mathbf{x}'-\mathbf{x}\right\rangle =\mathbf{t}=\underline{w}\left\langle \mathbf{x}'-\mathbf{x}\right\rangle \mathbf{P}\mathbf{K}^{-1}\left(\mathbf{x}'-\mathbf{x}\right) \tag{10}$$

where $\mathbf{K}$ is the shape tensor which is defined as

$$\mathbf{K}=\int_{H_{\mathbf{x}}}\underline{w}\left\langle \mathbf{x}'-\mathbf{x}\right\rangle\left(\underline{\mathbf{X}}\left\langle \mathbf{x}'-\mathbf{x}\right\rangle\otimes\underline{\mathbf{X}}\left\langle \mathbf{x}'-\mathbf{x}\right\rangle\right)dV' \tag{11}$$

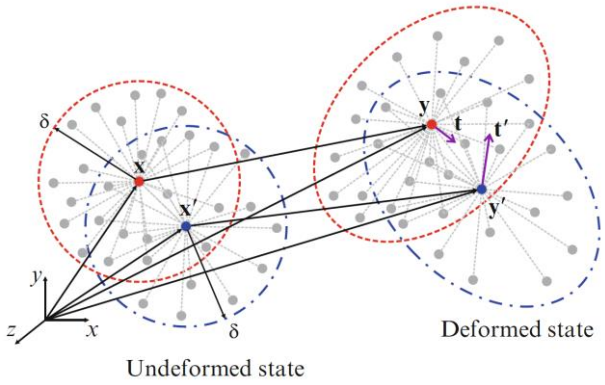

Figure 5. Non-ordinary state-based peridynamics

where $\underline{\mathbf{X}}\langle\bullet\rangle$ is the position state which contains the relative position of material points associated with a particular bond and $\underline{w}\langle\bullet\rangle$ state contains the influence function information which defines the strength of interactions.

In order to incorporate material models of CCM in peridynamics, it is essential to relate the stress components to associated strain components. The definition of deformation gradient will be necessary to calculate the strain tensor. The deformation gradient, **F**, can be approximated in peridynamic framework as

$$\tilde{\mathbf{F}} = \left[\int_{H_{\mathbf{x}}} \underline{w}\langle \mathbf{x}' - \mathbf{x} \rangle \left(\underline{\mathbf{Y}}\langle \mathbf{x}' - \mathbf{x} \rangle \otimes \underline{\mathbf{X}}\langle \mathbf{x}' - \mathbf{x} \rangle \right) dV' \right] \mathbf{K}^{-1} \tag{12}$$

where $\underline{\mathbf{Y}}\langle\bullet\rangle$ is the deformation state containing the relative position of bonds in the deformed configuration. Non-ordinary state-based peridynamics is a useful and practical approach. However, it encounters zero-energy mode problem and several techniques were proposed to overcome this problem [5]. In this study, the approach proposed by Silling [6] is used to remove the zero-energy mode problem by adding a stabilisation term to non-ordinary state-based peridynamic force term given in Eq. (10) as

$$\underline{\mathbf{T}}(\mathbf{x},t)\langle \mathbf{x}' - \mathbf{x} \rangle = \underline{w}\langle \mathbf{x}' - \mathbf{x} \rangle \left(\mathbf{P}\mathbf{K}^{-1}(\mathbf{x}' - \mathbf{x}) + \frac{Gc}{w_0 \delta} \underline{\mathbf{z}}\langle \mathbf{x}' - \mathbf{x} \rangle \right) \tag{13}$$

where G is a positive constant, c is the bond-based peridynamic bond constant given in Eq. (4), δ is the horizon size and w_0 is defined as

$$w_0 = \int_{H_{\mathbf{x}}} \underline{w}\langle \mathbf{x}' - \mathbf{x} \rangle \, dV' \tag{14}$$

$\underline{\mathbf{z}}$ in Eq. (13) is the nonuniform part of the deformation state which can be expressed as

$$\underline{\mathbf{z}}\langle \mathbf{x}' - \mathbf{x} \rangle = \underline{\mathbf{Y}}\langle \mathbf{x}' - \mathbf{x} \rangle - \tilde{\mathbf{F}}(\mathbf{x}' - \mathbf{x}) \tag{15}$$

Numerical implementation

Spatial integration

Solution of peridynamic equation of motion by using analytical techniques is usually not possible. Therefore, numerical techniques are utilized and meshless approach is widely used for this purpose. The solution domain is discretized into finite number of volumes and each volume can be represented by a point located at its center (Fig. 6). The peridynamic equation of motion in integral form can then be expressed in terms of a finite summation form as

$$\rho(\mathbf{x}_k)\ddot{\mathbf{u}}(\mathbf{x}_k,t)=\sum_{j=1}^{N_k}\{\mathbf{t}_{kj}-\mathbf{t}_{jk}\}V_j+\mathbf{b}(\mathbf{x}_k,t) \tag{16}$$

where N_k is the number of points inside the horizon of the material point *k*.

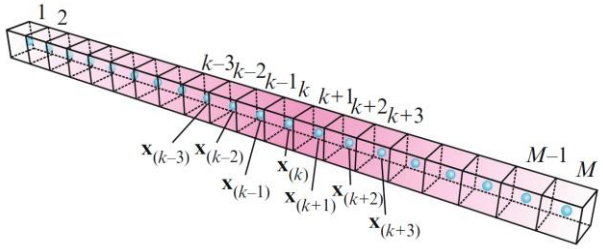

Figure 6. Meshless discretization

Dual Horizon Peridynamics for Non-uniform Discretisation and Variable Horizon

Peridynamic forces given in Eq. (16) can be written in terms of micropotentials between interacting material points, ω, as

$$\mathbf{t}_{kj}=\frac{1}{2}\frac{1}{V_j}\left(\sum_{i=1}^{N_k}\frac{\partial\omega_{ki}}{\partial(\mathbf{y}_j-\mathbf{y}_k)}V_i\right) \tag{17}$$

$$\mathbf{t}_{jk}=\frac{1}{2}\frac{1}{V_k}\left(\sum_{i=1}^{N_j}\frac{\partial\omega_{ji}}{\partial(\mathbf{y}_k-\mathbf{y}_j)}V_i\right) \tag{18}$$

where N_k and N_j represent the number of family members within the horizon of material points k and j. For ordinary-state based peridynamics, peridynamic forces can be rewritten for variable size horizon case as

$$\mathbf{t}_{kj}=\alpha_{kj}\left(\frac{2ad\delta}{|\mathbf{x}_j-\mathbf{x}_k|}\theta_k(\mathbf{x}_k,t)+bs_{kj}\right)\frac{\mathbf{y}_j-\mathbf{y}_k}{|\mathbf{y}_j-\mathbf{y}_k|} \tag{19}$$

$$\mathbf{t}_{jk}=\alpha_{jk}\left(\frac{2ad\delta}{|\mathbf{x}_j-\mathbf{x}_k|}\theta_j(\mathbf{x}_j,t)+bs_{kj}\right)\frac{\mathbf{y}_k-\mathbf{y}_j}{|\mathbf{y}_k-\mathbf{y}_j|} \tag{20}$$

with

$$\alpha_{kj} = \begin{cases} 1, \omega_{kj} \neq 0 \\ 0, \omega_{kj} = 0 \end{cases} \tag{21}$$

$$\alpha_{jk} = \begin{cases} 1, \omega_{jk} \neq 0 \\ 0, \omega_{jk} = 0 \end{cases} \tag{22}$$

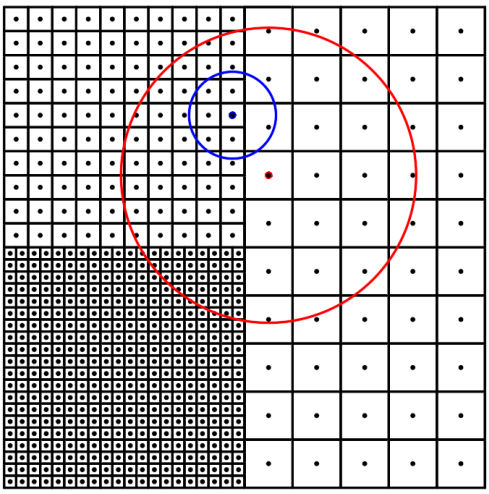

Figure 7. Non-uniform discretization with different horizon sizes.

Note that in Eqs. (21) and (22), the micropotential being zero means one of the material point is not within the horizon of the other material point (see Fig. 7). For non-ordinary state-based peridynamics, peridynamic forces for variable horizon can be expressed as

$$\mathbf{t}_{kj} = \alpha_{kj} \left\{ \underline{w} \langle \mathbf{x}_j - \mathbf{x}_k \rangle \mathbf{P}[\mathbf{x}_k] \mathbf{K}^{-1}[\mathbf{x}_k] (\mathbf{x}_j - \mathbf{x}_k) \right\} \tag{23}$$

$$\mathbf{t}_{jk} = \alpha_{jk} \left\{ \underline{w} \langle \mathbf{x}_k - \mathbf{x}_j \rangle \mathbf{P}[\mathbf{x}_j] \mathbf{K}^{-1}[\mathbf{x}_j] (\mathbf{x}_k - \mathbf{x}_j) \right\} \tag{24}$$

For bond-based peridynamics, peridynamic force between two interacting material points is only influenced by the motion of these two material points. In other words, only micropotentials which belong to both interacting points exist, i.e. $\omega_{ik} = \omega_{ki} = 0, \text{if } i \neq j$. Therefore, peridynamic forces given in Eqs. (17) and (18) can be simplified as

$$\mathbf{t}_{kj} = \frac{1}{2} \left(\frac{\partial \omega_{kj}}{\partial (\mathbf{y}_j - \mathbf{y}_k)} \right) \tag{25}$$

$$\mathbf{t}_{jk} = \frac{1}{2} \left(\frac{\partial \omega_{jk}}{\partial (\mathbf{y}_k - \mathbf{y}_j)} \right) \tag{26}$$

These forces can be expressed as

$$\mathbf{t}_{kj} = \alpha_{kj} (c s_{kj}) \frac{\mathbf{y}_j - \mathbf{y}_k}{|\mathbf{y}_j - \mathbf{y}_k|} \tag{27}$$

$$\mathbf{t}_{jk} = \alpha_{jk}\left(c\, s_{kj}\right)\frac{\mathbf{y}_k - \mathbf{y}_j}{\left|\mathbf{y}_k - \mathbf{y}_j\right|} \tag{28}$$

Since state-based peridynamic equation of motion given in Eq. (16) has two force components, each force component can be represented by a bond and each bond can break independently (see Fig. 8).

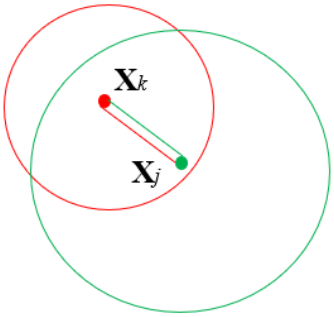

Figure 8. Schematic diagram for two different bonds between two material points.

Hence, for the stretch s_{kj} between two material points *k* and *j*, it can be written as

$$s_{kj} > s_c\left(\delta_k\right) \rightarrow \mathbf{t}_{kj} = 0 \tag{29}$$

and

$$s_{kj} > s_c\left(\delta_j\right) \rightarrow \mathbf{t}_{jk} = 0 \tag{30}$$

where δ_k and δ_j are horizon sizes of material points *k* and *j*, respectively. The critical bond stretch for two dimensional structures can be expressed in terms of horizon size as

$$s_c\left(\delta\right) = \sqrt{\frac{4\pi G_c}{9E\delta}} \tag{31}$$

Determination of Horizon Size Without Considering Damage and Nonlocal Effects

For the special condition that there is no existence of damage in the structure and non-local effects are insignificant, peridynamic solution should converge to the classical continuum mechanics solution as horizon size converges to 0 [2]. In this case, classical continuum mechanics solution can serve as a reference solution for peridynamics. Comparing peridynamic results against analytical and finite element method solutions will be sufficient to make decisions on the suitable value of horizon size. Several important aspects are explored to determine the horizon size for both constant and variable horizon sizes and uniform and non-uniform discretisation.

Horizon Size for Uniform Discretisation

In this task, we explore how to determine the optimum size of the horizon with respect to the grid spacing and the size of the solution domain for uniform discretization. Peridynamic equations are in the form of integro-differential equations and analytical solutions for such equations are limited. Therefore, numerical solution based on meshless discretization is a common practice. For simplicity, uniform discretization is utilized by dividing the solution domain into equal volumes with finite size and each volume is represented with a point located at its center. Therefore, in practice, it is not

possible to obtain a condition where horizon size becomes infinitely small. In such cases, Silling and Askari [7] suggested to use a horizon size equivalent to three times of the discretization size, i.e. smallest distance between two neighboring points based on their experience and observations of the results that they obtained using bond-based peridynamics (see Fig. 9).

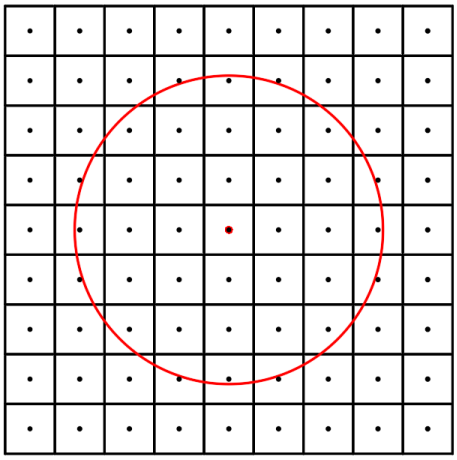

Figure 9. Meshless uniform discretization and horizon of a material point with a size equivalent to three times of the discretization size

To make decisions on the horizon size, there are several important aspects to be considered. The first one is to take into account sufficient number of interactions between material points to capture all possible deformation modes. For instance, if a material point is only interacting with its nearest neighbors except the ones located at its diagonals, it is not possible to capture shear deformation especially in bond-based peridynamic formulation. The second important aspect is the dependence of horizon size on the discretization size. Using smaller discretization size will increase the accuracy of the numerical calculations. However, this will also increase the computational time. Therefore, it is important to determine an optimum discretization size providing sufficient accuracy and leading to reasonable computational time. Since horizon size should be bigger than discretization size, achieving efficiency in computational time introduces additional restriction on the horizon size approaching to its ideal size, i.e. becoming infinitely small. Currently, a common approach is to perform m- and δ-convergence analysis by changing the discretization size and horizon size, respectively. However, since such convergence studies are time consuming especially for large scale problems, it is essential to determine a horizon size which can be safely used in all applications and leading to minimum computational time. Another important aspect is the nature of the problem being static or dynamic. It is necessary to determine if the same size of horizon is suitable for both conditions. Moreover, dynamic problems may experience unphysical wave reflection which can lead to inaccurate results as the waves are travelling inside the solution domain. Finally, it is important to investigate if the same horizon size is applicable for all 1-Dimensional (1-D), 2-Dimensional (2-D) and 3-Dimensional (3-D) models. Note that circular and spherical domains are commonly used for the shape of the horizon for 2-D and 3-D cases, respectively, which is considered for this part of the investigation. Moreover, both ordinary-state based and non-ordinary state-based formulations are utilised and it is important to

investigate if same horizon size can be used in both formulations. This investigation can also show if state-based formulations will have a different tendency with respect to bond-based formulations since in state-based peridynamic formulations the effect of family members are taken into account which is ignored in bond-based peridynamic formulation.

To determine the horizon size, first, simple geometries, boundary and loading conditions are considered under both static and dynamic conditions. To demonstrate the general applicability of the determined horizon sizes more complicated problem cases are considered. Finite element solutions for the same cases are also evaluated as a reference solution. Details of this analysis can be found in [8].

Horizon Size for Non-uniform Discretization

In this task, we explore how to determine the optimum size of the horizon that we can use at different parts of the solution domain for non-uniform discretization. Uniform discretization is simple and widely used in peridynamic simulations. However, for certain problems, uniform discretization becomes unfeasible such as a sub-region with a very small thickness. Moreover, as in the finite element simulations, it may be computationally advantageous to use different grid sizes at different parts of the domain (Fig. 7). Since grid size and horizon is directly related, it is essential to determine horizon sizes which can be applicable for these cases. Note that such a case is more prone to numerical errors. Details of this analysis can be found in [9]. An extension of dual-horizon peridynamic formulation to be used for thermal diffusion analysis is also developed as part of this task and presented in [10].

The Effect of Shape of the Horizon

In this task, we investigate the effect of the shape of the horizon. For the shape of the horizon, it is a general trend to choose a spherical domain for 3-Dimensional models and a circular domain for 2-Dimensional models. However, it is important to explore what happens if a different shape is chosen.

After determining a suitable horizon size for uniform and non-uniform discretizations for circular (2-D) and spherical (3-D) shaped horizons, we considered other horizon shapes including square and irregular shaped horizons (see Fig. 10). We investigate if any of these horizon shapes introduce numerical inaccuracies especially for dynamic problems which may cause unphysical wave reflections. Details of this analysis can be found in [11].

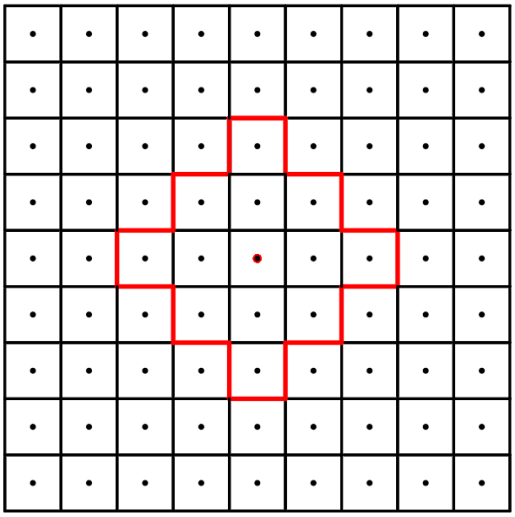

Figure 10. Horizons with irregular shapes.

Determination of Horizon Size by Considering Nonlocal Effects Without Damage Based on Dispersion Relationships

The equation of motion in bond-based peridynamic theory for the material point *x* can be written as

$$\rho\ddot{u}(x,t)=\int_V c(x'-x)\,s(u'-u,x'-x)\,dV \tag{32}$$

where x, x' are the coordinates of the paired material points, u', u are the displacements of the material points, $c(x'-x)$ is the bond constant, ρ is the mass density, $s(u'-u,x'-x)$ is the stretch of the paired material points, which can be expressed in 1-D as

$$s(u'-u,x'-x)=\frac{u'+x'-u-x}{|x'-x|} \tag{33}$$

The equation of motion can be solved with plane wave solution $u(x,t)$ as

$$u(x,t)=Ue^{i(kx-\omega t)} \tag{34}$$

where U is the constant amplitude vector, k is the wavenumber, ω is the angular frequency in rad/sec. Substituting the plane wave solution given in Eq. (34) in Eq. (32) leads to

$$\rho\omega_{pd}^2=2\int_0^{\delta}\frac{C(\xi)}{\xi}\left(1-\cos(k\xi)\right)A\,d\xi \tag{35}$$

where δ is the horizon size, A is the cross-sectional area, and $\xi=|x'-x|$. Bond constant for isotropic materials in a one-dimensional bar can be written as

$$C(\xi)=\frac{2E}{A\delta^2} \tag{36}$$

where E is the elastic modulus. Substituting the bond constant expression given in Eq. (36) in the peridynamic equation of motion with the plane wave solution given in Eq. (35), the analytical solution of the wave dispersion relationship for one-dimensional structures in terms of wave number and the horizon size can be obtained as

$$\omega_{pd}^2 = \frac{4E}{\rho\delta^2}\left(\gamma - \text{cosintegral}\left(k\delta\right) + \ln\left(k\delta\right)\right) \tag{37}$$

where γ is the Euler gamma constant. Note that dispersion of the peridynamic wave is only related to the micromodulus function, density, and horizon. These parameters are inherent properties of the material. Dispersion relationships for 2-Dimensional and 3-Dimensional problems, and state-based peridynamic formulations can be obtained similarly. For 2-Dimensional ordinary state-based formulation, the dispersion relationships in longitudinal and transverse directions can be written, respectively, as

$$\omega_L = \sqrt{16\frac{\left(\kappa - 2\mu\right)}{\rho\delta^4}\left[\frac{\left(1 - BesselJ\left[0, \delta\cdot k\right]\right)}{k}\right]^2 + 24\frac{\mu}{\rho\delta^3}\left(\delta - \frac{2BesselJ\left[1, \delta\cdot k\right]}{k}\right)} \tag{38}$$

$$\omega_{Tr} = \sqrt{24\frac{\mu}{\delta^3}\left(\delta - \frac{BesselJ\left[1, \delta\cdot k\right]\left(-2 + \delta\cdot k\cdot\pi\cdot \text{StruveH}\left[0, \delta\cdot k\right]\right)}{k} - \delta\cdot BesselJ\left[0, \delta\cdot k\right]\cdot\left(2 - \pi\cdot\text{StruveH}\left[1, \delta\cdot k\right]\right)\right)} \tag{39}$$

For 3-Dimensional ordinary state-based formulation, the dispersion relationships in longitudinal, transverse and vertical directions can be written, respectively, as

$$\omega_L = \sqrt{81\frac{\left(\kappa - \frac{5\mu}{3}\right)}{16\rho\pi^2\delta^6}\left[\int_0^{2\pi}\frac{\pi\,\text{Sec}\,\theta\,\text{StruveH}\left[0, \delta k\,\text{Cos}\,\theta\right] - \delta k\pi\,\text{StruveH}\left[-1, \delta k\,\text{Cos}\,\theta\right]}{k^2}d\theta\right]^2 - \frac{30\mu}{\rho\pi\delta^4}\frac{2\pi\left[-k\left(6 + \delta^2k^2 + 6\cos\left(\delta k\right)\right) + \frac{12\sin\left(\delta k\right)}{\delta}\right]}{3k^3}} \tag{40}$$

$$\omega_{Tr} = \sqrt{\frac{30\mu}{\rho\pi\delta^4}\int_0^{2\pi}\frac{\left(2 - \pi\text{StruveH}\left[-1, \delta k\,\text{Cos}\,\theta\right] - \pi\text{StruveH}\left[1, \delta k\,\text{Cos}\,\theta\right] + \delta k\pi\,\text{Cos}\,\theta\,\text{StruveH}\left[2, \delta k\,\text{Cos}\,\theta\right]\right)\text{Tan}^2\,\theta}{k^2}d\theta} \tag{41}$$

$$\omega_{Vr} = \sqrt{\frac{30\mu}{\rho\pi\delta^4}\frac{2\pi\left(-6\delta k + \delta^3 k^3 + 6\sin\left(\delta k\right)\right)}{3\delta k^3}} \tag{42}$$

Peridynamic horizon size can be obtained by comparing peridynamic dispersion relationships with the dispersion relationships obtained from experiments or lattice dynamic models. The details of the derivation of peridynamic dispersion relationships can be obtained in [12,13].

Determination of Horizon Size by Considering Damage

Stress intensity factor

Irwin found that the stresses around a crack could be expressed in terms of a scaling factor called the stress intensity factor. The stress intensity factor, *K*, is used in fracture mechanics to predict the stress state ("stress intensity") near the tip of a crack or notch caused by a remote load or residual stresses. The magnitude of *K* depends on *specimen geometry, the size and location of the crack or notch*, and the *magnitude and the distribution of loads* on the material.

For Mode I opening mode, a tensile stress is normal to the plane of the crack and the crack surfaces move directly apart. The stress intensity factor for an infinite size plate and Mode I condition is given as

$$K = \sigma\sqrt{\pi a} \tag{43}$$

while the form of stress intensity factor for a finite size plate can be written as

$$K = \sigma\sqrt{\pi a}\, f\left(a/b\right) \tag{44}$$

where σ is the applied tension stress, a is the half width of the crack, and b is the half width of the finite plate. $f\left(a/b\right)$ is a function in terms of width of the crack and width of the finite plate, one of the suggested functions is provided as

$$f\left(a/b\right) = \frac{1 - \frac{a}{2b} + 0.326\left(\frac{a}{b}\right)^2}{\sqrt{1-\frac{a}{b}}} \tag{45}$$

The relationship between $f\left(n\right)$ and $n = b/a$ is presented in Fig. 11.

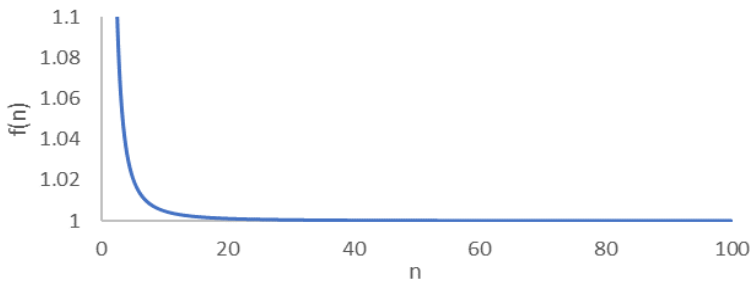

Figure 11. Variation of $f\left(n\right)$ with $n = b/a$.

As can be observed from Fig. 11, the function reaches close to a constant value of 1 when $n>10$. Thus, $b>10a$ can offer a suitable numerical domain model to represent infinite plate. In this occasion, $b=20a$ is adopted.

Griffith crack

An elastic plate with a line crack, located at $-l<x<l, y=0$ and subjected to a uniform tension loading $\tau_{yy}=\tau_0$ at infinity, is known as the Griffith crack (see Fig. 12).

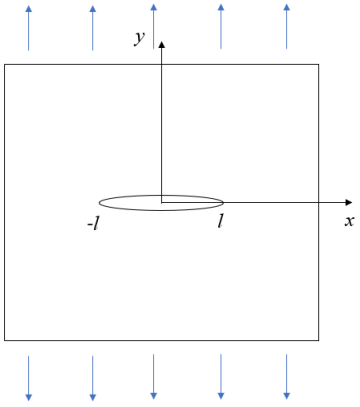

Figure 12. Griffith crack problem.

It is reported that the maximum nonlocal stress predicted by the nonlocal theory occurs slightly away from the crack tip [14]. According to a lattice model [15] and with computer simulations [16], this result is also confirmed. In this study, the horizon size at the crack tip is determined by comparing the stress field at the crack tip obtained from peridynamics and non-local elasticity.

Stress evaluation by using peridynamics

Stress evaluation in peridynamics can be summarized as:

Step 1 : The deformation gradient tensor, **F**, in peridynamic is defined as

$$\mathbf{F}=\left[\int_H \underline{w}(\boldsymbol{\xi})\underline{Y}(\boldsymbol{\xi})\times\boldsymbol{\xi}\,dV_{\xi}\right]\mathbf{K}^{-1} \tag{45}$$

where $\underline{w}(\boldsymbol{\xi})$ is the weight function, $\underline{Y}(\boldsymbol{\xi})$ is the bond vector between two material points in the deformed configuration, $\boldsymbol{\xi}$, is the bond vector between two material points in the undeformed configuration, and $\mathbf{K}$ is the shape tensor, which is defined as

$$\mathbf{K}=\left[\int_H \underline{w}(\boldsymbol{\xi})\boldsymbol{\xi}\times\boldsymbol{\xi}\,dV_{\xi}\right] \tag{46}$$

Step 2 : In classical theory, the Green-Lagrange strain tensor can be written as

$$\mathbf{E} = \frac{1}{2}\left(\mathbf{F}^T\mathbf{F} - \mathbf{I}\right) \tag{47}$$

Step 3 : The Second Piola-Kirchhoff (Kirchhoff) stress tensor $\mathbf{S}$ can be obtained as

$$\mathbf{S} = \mathbf{C}\mathbf{E} \tag{48}$$

where $\mathbf{C}$ is the stiffness matrix

Step 4 : Second Piola-Kirchhoff (Kirchhoff) stress tensor $\mathbf{S}$ in terms of the Cauchy stress $\boldsymbol{\sigma}$ can be written as

$$\mathbf{S} = J\mathbf{F}^{-1}\boldsymbol{\sigma}\mathbf{F}^{-T} \tag{49}$$

where J is the determinant of $\mathbf{F}$

Step 5: The Cauchy stress $\boldsymbol{\sigma}$ can be achieved as

$$\boldsymbol{\sigma} = \frac{1}{J}\mathbf{F}\mathbf{S}\mathbf{F}^T \tag{50}$$

Crack Tip Damage Zone Investigation

A domain T around crack tip C shown in Fig. 13 is created with a length $L = 6\times10^{-9}\ \mathrm{m}$ and width $W = 6\times10^{-9}\ \mathrm{m}$. The T field is discretized with 4δ in length and 4δ in width, where δ is the horizon size with $\delta = n\Delta x$, $n = 3, 6, 12, 24$, and Δx represents the spacing between material points. To allow material points at the edge of the T domain to interact with its family of material points, the domain T is wrapped with a boundary layer of δ. An example of the domain discretization is also shown in Fig. 13.

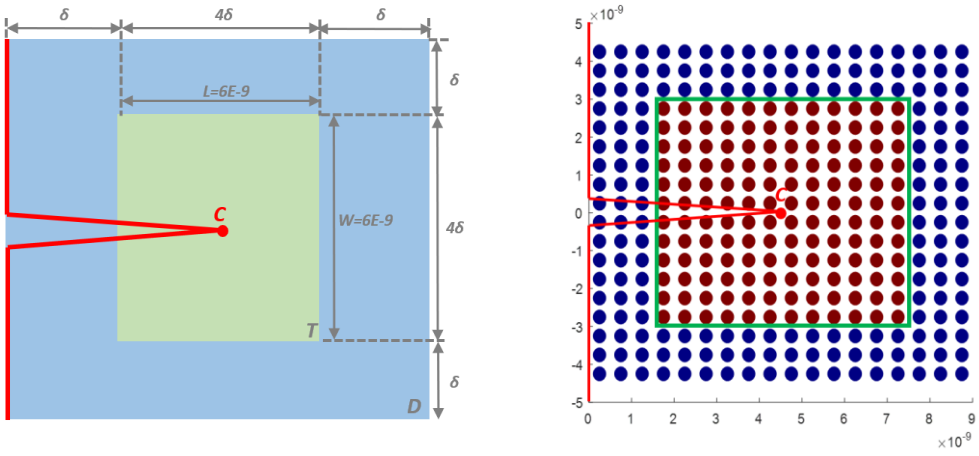

Figure 13. Crack tip region and the discretization

The analytical solution for displacement fields around the tip of a slit-like plane crack in an ideal

Hookean continuum solid for Mode-I loading is given as

$$\begin{Bmatrix} u_x \\ u_y \end{Bmatrix} = \frac{K}{E}\sqrt{\frac{r}{2\pi}} \begin{Bmatrix} (1+\nu)\left[(2k-1)\cos\left(\frac{\theta}{2}\right) - \cos\left(\frac{3\theta}{2}\right)\right] \\ (1+\nu)\left[(2k+1)\sin\left(\frac{\theta}{2}\right) - \sin\left(\frac{3\theta}{2}\right)\right] \end{Bmatrix} \tag{51}$$

In plane stress condition,

$$k = \frac{3-\nu}{1+\nu} \tag{52}$$

K is the stress intensity factor, E is the Young's modulus, r , θ are the distance and angle from the crack tip, respectively, ν is the Poisson's ratio. The stress intensity factor *K* determines the intensity of the local field and depends on the applied loading and specimen geometry. The remaining factors depend only on the spatial coordinates about the crack tip. It is assumed that $K = 1$. Defining a quantity G called the mechanical-energy-release rate, the relationship between stress intensity factor *K* and mechanical-energy-release rate for the described crack model can be represented as

$$G = \frac{K_I^2}{E} \tag{53}$$

In peridynamic framework, the bond is broken once the stretch between two material points exceeds the critical stretch. The material properties are specified as $E = 1\text{Pa}$ and $\nu = 1/3$.

The displacement fields and stretches at several spacing arrangements, $\delta = n\Delta x$, $n = 3, 6, 12, 24$ are examined. The size of the horizon is fixed in each scenario, while the mesh configuration is refined with increasing n.

Determination of Horizon Size Based on The Plasticity Field Around Crack Tip

The horizon size can also be determined based on the plasticity field around the crack tip by calculating the stresses at the crack tip. For a 2-Dimensional model, the stiffness matrix can written as

$$\mathbf{C} = \begin{bmatrix} \kappa+\mu & \kappa-\mu & 0 \\ \kappa-\mu & \kappa+\mu & 0 \\ 0 & 0 & \mu \end{bmatrix} \tag{54}$$

in which κ is bulk modulus and μ is shear modulus and for two-dimensional models, they are defined as

$$\kappa = \frac{E}{2(1-\nu)} \tag{55}$$

and

$$\mu = \frac{E}{2(1+\nu)} \tag{56}$$

where E is Young's Modulus.

The stress state has three normal stresses $\sigma_{xx}, \sigma_{yy}, \sigma_{zz}$ and three independent shear stresses $\tau_{yz}, \tau_{zx}, \tau_{xy}$. The stress field is defined in vector form as

$$\boldsymbol{\sigma} = \begin{bmatrix} \sigma_{xx} & \sigma_{yy} & \sigma_{zz} & \tau_{yz} & \tau_{zx} & \tau_{xy} \end{bmatrix}^T \tag{57}$$

Under plane stress assumption, the thin flat plate is subject to in-plane forces only and the stresses in the thickness direction vanishes, i.e.

$$\sigma_{zz} = \tau_{yz} = \tau_{zx} = 0 \tag{58}$$

Therefore, the von Mises stress in plane stress condition can be calculated as

$$\sigma_{VM} = \sqrt{\sigma_{xx}^2 - \sigma_{xx}\sigma_{yy} + \sigma_{yy}^2 + 3\tau_{xy}^2} \tag{59}$$

Multi-horizon Peridynamic Formulation

When the size of the horizon increases, the contribution of the Taylor expansion remainder related to the numerical procedure becomes significant. When the analysis is under requirement of high precision, ignoring remainders inappropriately may lead the results to deviate from expected results. The errors, which are dominated by remainders, are in direct proportion to the distance between the main material point and its family members. In other words, decreasing the horizon size will enhance accuracy. However, adopting this measure will reduce the nonlocal characteristic of the PD function. Moreover, for the numerical analysis, decreasing the horizon size suggests more material points are required as part of discretization and the computational time can high.

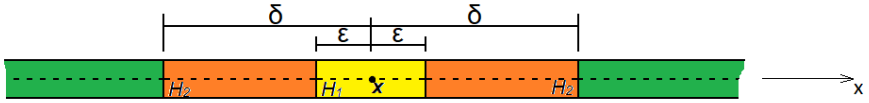

Figure 14. Multi-horizon for one-dimensional structures

In this section, a multi-horizon approach is introduced, which not only ensures the accuracy the PD function, i.e. decreases the effect of the Taylor expansion remainder as mentioned above, but also keeps the nonlocal characteristic of the PD function and achieve reasonable computational time in numerical analysis. More specifically, the family of the PD material point, $H_{\mathbf{x}}$, is constructed by two horizons, H_1 and H_2, as shown in Fig. 14. Here, the choice of the size of the total horizon, δ, has no limit, and the horizon size of H_1, ε, is suggested to be a small value. The purpose of

introducing a small horizon, H_1, is to ensure the errors of bond forces in this region, which are generated by Taylor expansion remainder, are negligibly small. The errors of bond forces in region H_2 are corrected at a similar small degree with those in region H_1 by a kernel function. According to this approach, the final form of the PD function can be written as

$$\rho\ddot{\mathbf{u}}(\mathbf{x},t) = w_1 \int_{H_1} \mathbf{t}(\mathbf{x}) dH_1 + w_2 \int_{H_2} k \cdot \mathbf{t}(\mathbf{x}) dH_2 + \mathbf{b}(\mathbf{x}) \tag{60}$$

where $\mathbf{t}(\mathbf{x})$ is the bond force density vector, w_1 and w_2 are the weight function for horizon H_1 and H_2, respectively, which are required to satisfy normalization condition as

$$w_1 + w_2 = 1 \tag{61}$$

The values of the weight functions are related with the proportion of their horizon size in the total horizon. Note that if $w_2 = 0$, Eq. (60) will reduce to the classical PD function; if $w_1 = 0$, the PD horizon will become an annular region and the main PD material point looses interactions with the material points in the inner region, H_1.

Surface Elasticity

In nano-materials, material properties close to the surfaces can be different than bulk properties. This variation causes surface stresses. In this study, modified core-shell model (MC-S) is utilised to define the variation of material properties in the surface region. Based on the MC-S model [17], for a rectangular nanowire, an exponential increase of surface elasticity in the surface between the bulk region and the surface region is assumed to have no jump by using following expression of surface elasticity that describes this behaviour as:

$$E_s(y) = E_{bulk} e^{(\alpha(y - W_b))}, \quad W_b \le y \le W_b + W_s \tag{62}$$

where E_{bulk} is the bulk elasicity of the rectangular nanowire and α is the surface factor related to surface thickness W_s as $\alpha = \tilde{\alpha} / W_s$ where $\tilde{\alpha}$ is the dimensionless constant which represents the degree of inhomogeneity transitioning from the bulk region to the external surface layer and its sign (positive or negative) describes the stiffening or softening of the surface layer.

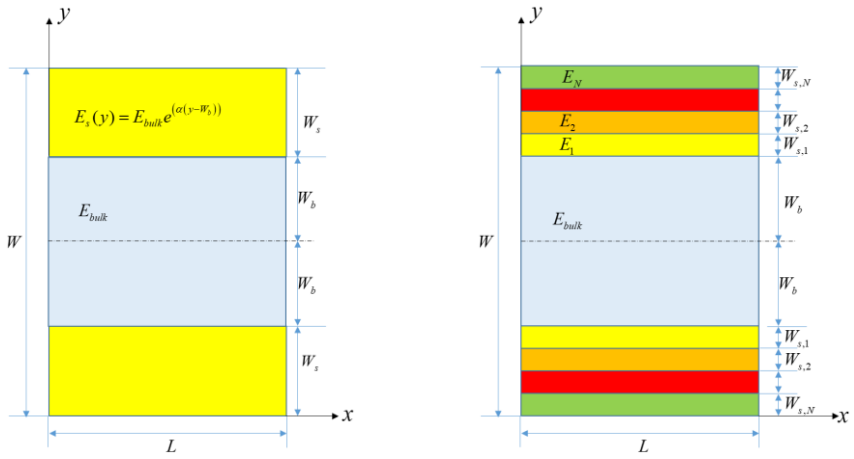

Figure 15. a) continuous model b) discrete model

The equivalent elastic modulus in the longitudinal direction with surface effects can be found by using static theory of elasticity for the continuous model (see Fig. 15a) when the plate is subjected to constant strain in the x direction:

$$E_{eq} = E_{bulk}\left(\frac{W_b}{(W_s + W_b)}\right) + \frac{E_{bulk}}{\alpha}\left(\frac{e^{(\alpha W_s)} - 1}{(W_s + W_b)}\right) \tag{63}$$

Similarly, the equivalent elastic modulus in the longitudinal direction with surface effects can be found by using static theory of elasticity for the discrete model (see Fig. 15b) when the plate is subjected to constant strain in the x direction:

$$E_{eq} = E_b \frac{(W_b)}{(W_s + W_b)} + \frac{\sum_{i=1}^{N} E_i W_i}{(W_s + W_b)} \tag{64}$$

with

$$E_i = E_{bulk} e^{(\alpha(y_i - W_b))}, \quad W_b \le y_i \le W_b + W_s \tag{65}$$

The equivalent elastic modulus in the transverse direction with surface effects can be found by using static theory of elasticity for the continuous model when the plate is subjected to constant stress in the y direction:

$$\frac{1}{E_{eq}} = \frac{1}{E_{bulk}} \frac{(W_b)}{(W_s + W_b)} - \frac{1}{E_{bulk}} \frac{\left(e^{-(\alpha W_s)} - 1\right)}{\alpha (W_s + W_b)} \tag{66}$$

Similarly, the equivalent elastic modulus in the transverse direction with surface effects can be found by using static theory of elasticity for the discrete model when the plate is subjected to constant stress in the y direction:

$$\frac{1}{E_{eq}} = \frac{1}{E_b} \frac{(W_b)}{(W_s + W_b)} + \frac{\sum_{i=1}^{N} \frac{1}{E_i} W_i}{(W_s + W_b)} \tag{67}$$

with

$$E_i = E_{bulk} e^{(\alpha(y_i - W_b))}, \quad W_b \le y_i \le W_b + W_s \tag{68}$$

The details of peridynamics surface elasticity formulation based on modified core-shell model (MC-S) can be found in [18].

A Computational Homogenization Framework for Non-Ordinary State-Based Peridynamics

The homogenization procedure developed in this work is a two-scale scheme: a microscopic scale represented by a Representative Volume Element (RVE), and a macroscopic scale represented by a homogeneous effective medium. The constitutive law of the microscale model is assumed to be explicitly known at every point of the micro-domain while the constitutive law of the micromodel is not known everywhere. The objective is to retrieve a constitutive law of the macroscale substitute medium from a numerical solution of an initial volume constraint problem (IVCP) at the level of the underlying microstructure. In this multiscale framework, an RVE is assigned to each integration point of the macro continuum. A peridynamic equilibrium solution of the RVE is sought using boundary condition generated by the macroscale deformation gradient. The solution of the RVE IVCP yields the microscale stress field which is then homogenized to produce macroscale stresses and associated material tangent tensor. The coupling of the micro and macro scale is achieved through averaging relationships and the energetic equivalence statement of the Hill-Mandel micro-homogeneity condition.

Consider a heterogeneous medium B^0 with characteristic size of heterogeneities to be l_{hetro}. Momentarily, let this medium be replaced by a homogeneous 'effective' medium B^h. The original heterogeneous medium is the microscale, and the geometrical arrangement and material characteristics of the heterogeneities constitute the microstructure while the effective medium is the macroscale. Define a grid on B^h and let each point $\bar{\mathbf{x}}$ on this grid be associated with a neighborhood Ω_s. Let Ω_s be bounded by a region Ω_c of positive volume in $\mathbb{R}^n$. Let a sample of B^h occupying the regions Ω_s and Ω_c be denoted as Ω_s^0 and Ω_c^0, respectively. Also, let a sample of B^0 occupying Ω_s be denoted as Ω_s^0 as shown in Fig. 16.

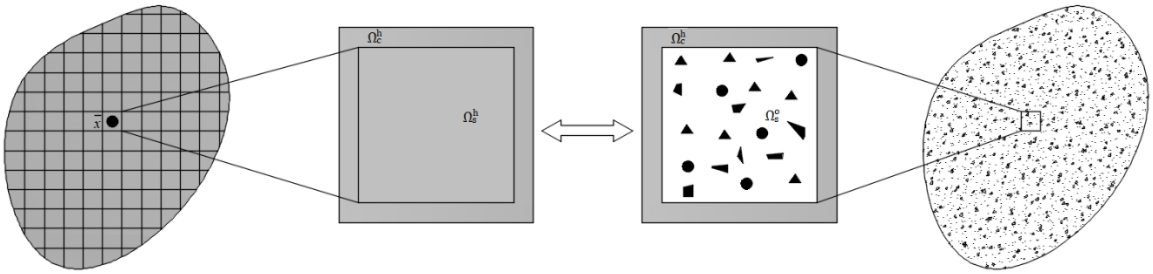

Figure 16. Homogenisation process.

Now, define a grid on Ω_s and let the position of points on this grid in the reference configuration be denoted as $\mathbf{x}$. The grid associated with $\bar{\mathbf{x}}$ is called the macroscale and the grid associated with $\mathbf{x}$ is the microscale. Let the characteristic lengths associated with the macroscale and the microscale be l_{macro} and l_{micro}, respectively. The morphology and material properties of the constituents of B^0 in the microscale are called the microstructure of B^h. If Ω_s^0 exists such that

$$l_{hetro} << l_{micro} << l_{macro} \tag{69}$$

then Ω_s^0 is referred to as an RVE associated with the macro point $\bar{\mathbf{x}}$ where Eq. (69) is the statement of the principle of separation of scale. This principle requires that the scale of the microstructure (or fluctuation of micro field such as stress and strain) should be much smaller than the size of the RVE considered which in turn should be much smaller than the characteristic length scale of the macro domain (or fluctuation of macro field variables).

Let B^h be subjected to an affine deformation at its boundary. This will produce a homogeneous strain $\bar{\boldsymbol{\varepsilon}}$ (for small deformation). This homogeneous strain will in turn generate a homogeneous stress field $\bar{\boldsymbol{\sigma}}$ everywhere in B^h. For simplicity, we will assume linear elastic material response in both scales, then the material model that relates $\bar{\boldsymbol{\sigma}}$ and $\bar{\boldsymbol{\varepsilon}}$ given by the generalised Hooke's law

$$\bar{\boldsymbol{\sigma}} = \mathbf{C}^* \bar{\boldsymbol{\varepsilon}} \quad \text{or} \quad \bar{\boldsymbol{\varepsilon}} = \mathbf{S}^* \bar{\boldsymbol{\sigma}} \tag{70}$$

is the effective or homogenised constitutive law, where $\mathbf{C}^*$ and $\mathbf{S}^*$ are the effective stiffness and compliance tensors, respectively. At the microscale, the constitutive relation in each phase of the microscale is given by

$$\boldsymbol{\sigma}(\mathbf{x}) = \mathbf{C}(\mathbf{x})\boldsymbol{\varepsilon}(\mathbf{x}) \text{ or } \boldsymbol{\varepsilon}(\mathbf{x}) = \mathbf{S}(\mathbf{x})\boldsymbol{\sigma}(\mathbf{x}) \tag{71}$$

If the condition for the existence of the RVE is satisfied (henceforth, this condition will be assumed to be satisfied), then the microscopic deformation will be assumed to admit the following decomposition:

$$\mathbf{u}(\mathbf{x}) = \bar{\boldsymbol{\varepsilon}}(\mathbf{x})\mathbf{x} + \mathbf{u}^*(\mathbf{x}) \text{ or } \boldsymbol{\varepsilon}(\mathbf{x}) = \bar{\boldsymbol{\varepsilon}} + \boldsymbol{\varepsilon}^* \tag{72}$$

where $\mathbf{u}^*$ and $\boldsymbol{\varepsilon}^*$ are the displacement and strain fluctuation due to the presence of the microstructure, respectively. Details of this analysis can be found in [19].

Static Condensation of The Peridynamic Heat Conduction Model

Peridynamic heat conduction model can be expressed in the discrete form as:

$$\dot{\tau} = \sum_{i=1}^{N} K\left(\tau_j - \tau_i\right) V_j + h_i \tag{73}$$

where $\dot{\tau} = \dfrac{\partial \tau_i}{\partial t}$ and N is the number of nodes in the neighbourhood of node i.

The assembled peridynamic transient heat conduction equations for the body in matrix form is given

by:

$$\mathbf{I}\dot{\tau}+\mathbf{K}\tau=h \tag{74}$$

where $\mathbf{I}$ and $\mathbf{K}$ are the identity and diffusivity modulus matrices respectively and n is the total degrees of freedom in the system. In this context, Eq. (74) is referred to as the *full order model* of the system or simply *full model*. The objective of the model reduction is to replace the full model having n degree of freedom with a reduced order system having m degree of freedom, such that $m \ll n$. The reduced model is expected to preserve the heat conduction characteristics of the full model. To proceed with the model condensation, the degree of freedom of the system are separated into retained and truncated degrees of freedom. The retained degrees of freedom are those to be preserved while truncated degrees of freedom are those to be condensed out in the reduced model. Let r denote the retained degrees of freedom and let t denote the truncated degrees of freedom, then Eq. (74) can be partitioned as follows:

$$\begin{bmatrix}\mathbf{I}_{rr} & \mathbf{I}_{rt}\\ \mathbf{I}_{tr} & \mathbf{I}_{tt}\end{bmatrix}\begin{Bmatrix}\dot{\boldsymbol{\tau}}_r\\ \dot{\boldsymbol{\tau}}_t\end{Bmatrix}+\begin{bmatrix}\mathbf{K}_{rr} & \mathbf{K}_{rt}\\ \mathbf{K}_{tr} & \mathbf{K}_{tt}\end{bmatrix}\begin{Bmatrix}\boldsymbol{\tau}_r\\ \boldsymbol{\tau}_t\end{Bmatrix}=\begin{Bmatrix}\mathbf{h}_r\\ \mathbf{h}_t\end{Bmatrix} \tag{75}$$

Neglecting the transient term and assuming there is no heat source at the truncated degrees of freedom, then the solution of the second submatrix equation for $\boldsymbol{\tau}_t$ yields

$$\boldsymbol{\tau}_t=\mathbf{R}_G\boldsymbol{\tau}_r \tag{76}$$

where $\mathbf{R}_G$ is the condensation matrix, defined as

$$\mathbf{R}_G=-\mathbf{K}_{tt}^{-1}\mathbf{K}_{tr} \tag{77}$$

The condensation matrix relates the retained degrees of freedom and truncated degrees of freedom and is load independent because it is assumed there is no heat source at the truncated degrees of freedom. Also note that in arriving at Eq. (76), the transient term in Eq. (75) have been neglected, hence this method is called static condensation method. The temperature state of the full model may be expressed as

$$\boldsymbol{\tau}=\begin{Bmatrix}\boldsymbol{\tau}_r\\ \boldsymbol{\tau}_t\end{Bmatrix}=\mathbf{T}_G\tau_r \tag{78}$$

where $\mathbf{T}_G$ is a transformation matrix given by:

$$\mathbf{T}_G=\begin{bmatrix}\mathbf{I}\\ \mathbf{R}_G\end{bmatrix} \tag{79}$$

If the transformation matrix is assumed to be independent of time, differentiating Eq. (78) with respect to time gives:

$$\dot{\boldsymbol{\tau}}=\mathbf{T}_G\dot{\boldsymbol{\tau}}_r \tag{80}$$

Substituting Eqs. (79) and (80) into Eq. (74) and pre-multiplying by $\mathbf{T}_G^T$ yields

$$\mathbf{I}_G\dot{\boldsymbol{\tau}}_r + \mathbf{K}_G\boldsymbol{\tau}_r = \mathbf{h}_G \tag{81}$$

where $\mathbf{I}_G$, $\mathbf{K}_G$ and $\mathbf{h}_G$ are the *reduced identity matrix*, *reduced diffusivity matrix* and *reduced load vector* respectively associated with the reduced model, defined as

$$\mathbf{I}_G = \mathbf{T}_G^T\mathbf{I}\mathbf{T}_G,\ \ \mathbf{K}_G = \mathbf{T}_G^T\mathbf{K}\mathbf{T}_G,\ \ \mathbf{h}_G = \mathbf{T}_G^T\mathbf{h} \tag{82}$$

Details of this analysis can be found in [20].

Results and Discussion:

Since numerous results are generated to determine the optimum horizon size and shape for peridynamics, several important observations are summarized and discussed in this section.

Determination of Horizon Size Without Considering Damage and Nonlocal Effects

For the case without considering damage and non-local effects, first, uniform discretization is utilized to discretize the solution domain and several benchmark problems are considered including vibration of a plate (2-D), plate under tension (2-D), vibration of a 3-Dimensional block (3-D) and block under tension loading (3-D). Hence, both dynamic and static conditions are explored. Solutions are obtained by using bond-based, ordinary state-based and non-ordinary state-based peridynamics. 2-Dimensional and 3-Dimensional analysis show similar behavior which is expected since peridynamic formulation is based on interactions between material points and 2-D or 3-D analysis is based on same form of calculations. Dynamic analysis and static analysis results also yield similar conclusions about the horizon size selection. Based on numerical results, it is confirmed that horizon size of $\delta = 3\Delta x$ (Δx is the discretization size) is an optimum horizon size for bond-based peridynamic analysis as Silling and Askari [7] suggested earlier. For ordinary-state based peridynamic analysis, same horizon size, i.e. $\delta = 3\Delta x$ is also obtained as the optimum horizon size. Although bond-based peridynamics is a special case of ordinary-state based peridynamics, the outcome is not intuitive since the peridynamic force in ordinary-state based peridynamics is dependent on motions of family members rather than only motions of interacting material points as in bond-based peridynamics formulation. For non-ordinary state-based peridynamics, it was concluded that $\delta = 2\Delta x$ is the most optimum choice for horizon size. This will result in significant reduction in computational time especially for 3-Dimensional analysis since there are much less material points inside a horizon of $\delta = 2\Delta x$ than a horizon with a size of $\delta = 2\Delta x$. Based on the numerical results, it should also be noted that for non-ordinary state-based formulation the horizon should be small since the non-ordinary state based model used in this study, i.e. correspondence model, has a direct connection with classical (local) continuum mechanics and requires determination of deformation gradient in peridynamic framework as the first step.

After determining optimum horizon sizes for all three peridynamic formulations, the performance of these horizon sizes is investigated for non-uniform discretization by considering the same benchmark problems for the uniform discretization analysis. By considering different scenarios having refined discretization on one side of the domain with same or different horizon size, it is

concluded that horizon sizes with the variable horizon peridynamic formulation presented in this report do not show significant change with respect to uniform discretization results. However, it should be noted that if there are more material points within a horizon, it reduces the numerical error due to numerical integration and leads to a more accurate solution. On the other hand, if the horizon size is getting larger and larger, the local behavior starts transforming into a non-local behavior which suggests that using a large horizon size with respect to the size of the solution domain is not suitable for problems showing classical (local) behavior. Moreover, if different horizon sizes are used in the solution domain, lack of interactions can introduce numerical error. In our numerical tests, it is observed that the effect of this numerical error is small. In addition, Dual Horizon Peridynamic formulation is developed for thermal diffusion analysis. Dual Horizon Peridynamics allows utilization of variable discretization and horizon size inside the computational domain which can bring significant advantages to peridynamic simulations in terms of computational time. To demonstrate the capability of the Dual Horizon Peridynamics formulation, three different example problems are considered including a square plate with temperature and no flux boundary conditions, a square plate under thermal shock loading, and a square plate with an insulated crack. For each of these problems, the solution domain is divided into two regions which can have different discretization and horizon sizes. Five different horizon sizes are considered to see the effect of the horizon size. For all the problems that are considered, good agreement is obtained between PD predictions and FEM results. If different discretization size or horizon size is utilized in different regions, a slight difference can be observed between PD and FEM results at the interface between the two regions and the difference increases as the horizons size increases. Hence, it can be concluded that presented Dual Horizon Peridynamic analysis can be effectively utilized for problems with different discretization and horizon sizes.

Next, the shape of the horizon size is investigated by considering circular, square and irregular shaped horizons. Based on the numerical tests, it is observed that square horizon is not very suitable for bond-based and ordinary-state based analysis. On the other hand, non-ordinary state based formulation is not sensitive to the shape of the horizon which suggests that any suitable shape for convenience can be used. As mentioned earlier, since 2-D and 3-D peridynamic analysis show similar behavior, it is expected that same trend can be observed for 3-Dimensional configurations.

The suggested horizon sizes are checked by considering more complex problems and comparison against reference FEM solution shows that suggested horizon sizes can provide accurate solutions with the advantage of computational efficiency.

Determination of Horizon Size by Considering Nonlocal Effects Without Damage Based on Dispersion Relationships

For the case with considering non-local effects and without damage, optimum horizon sizes for different materials including copper, gold, silver and platinum are obtained by comparing peridynamic dispersion curves against dispersion curves obtained either experimentally or from lattice model. Therefore, the obtained peridynamic ordinary state based dispersion relations given in Eqs.

(40-42) have been tested for copper, gold, platinum, silver and compared with the experimental data to determine the horizon size values for these materials. As shown in Fig. 17, the horizon size values for copper, gold, platinum, silver are determined as $\delta = 2.472\times10^{-10}\,\mathrm{m}$, $2.432\times10^{-10}\,\mathrm{m}$, $2.587\times10^{-10}\,\mathrm{m}$ and $2.894\times10^{-10}\,\mathrm{m}$, respectively.

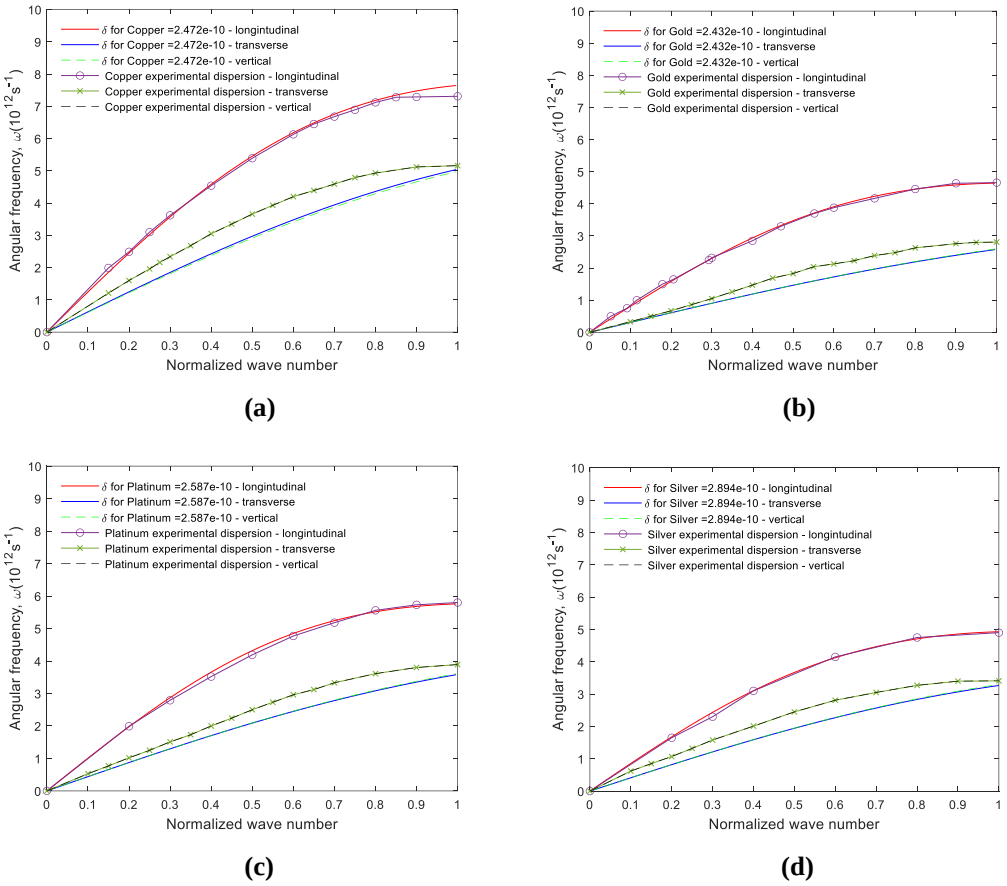

Figure 17. Dispersion relationships (a) copper, (b) gold, (c) platinum, (d) silver

Determination of Horizon Size by Considering Damage

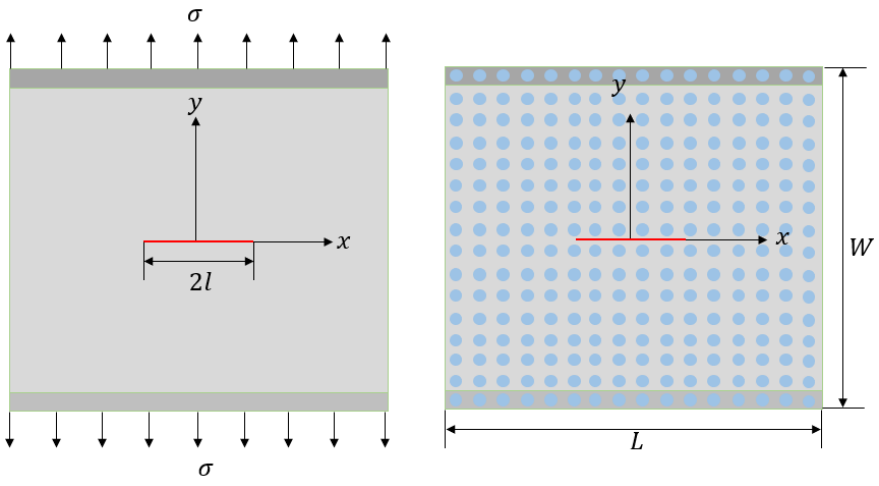

Figure 18. Plate with a central crack (Griffith crack problem).

In this study, the horizon size at the crack tip region is evaluated by comparing stress field obtained from peridynamics and nonlocal elasticity [14]. To demonstrate the process, a 2-Dimensional copper plate with a central crack is considered as shown in Fig. 18. The atomic distance for copper is $a = 3.598\times10^{-10}\,\mathrm{m}$. The material properties of copper are specified as; mass density, $\rho = 8960\,\mathrm{kg/m^3}$, elastic modulus, $E = 1.3\times10^{11}\,\mathrm{Pa}$ and Poisson's ratio, $\nu = 1/3$. The applied tension loading is $200\,\mathrm{MPa}$. For the plate dimensions of $L = W = 600a$, a central crack size of $2l = 100a$, and the horizon size of $\delta = 1.085\times10^{-9}\,\mathrm{m}$, the comparison of the vertical stress along the central *x*-axis is presented in Fig. 19.

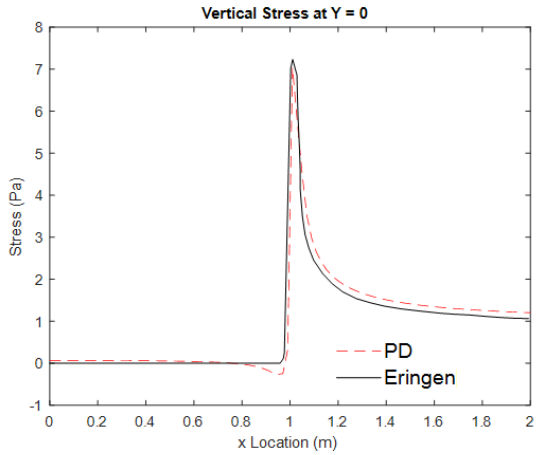

Figure 19. Comparison of the vertical stress along the central *x*-axis between peridynamics (PD) and nonlocal elasticity (Eringen [14]) solutions.

Based on the maximum dimensionless stress at the crack tip defined by Eringen et. al. [14], the maximum stress values at the crack tip for various crack sizes $2l = 20a, 40a, 60a, 80a, 100a$ obtained from peridynamics and nonlocal elasticity are compared in Fig. 20. As can be seen in this figure, a very good agreement is observed between the two solutions for different crack sizes.

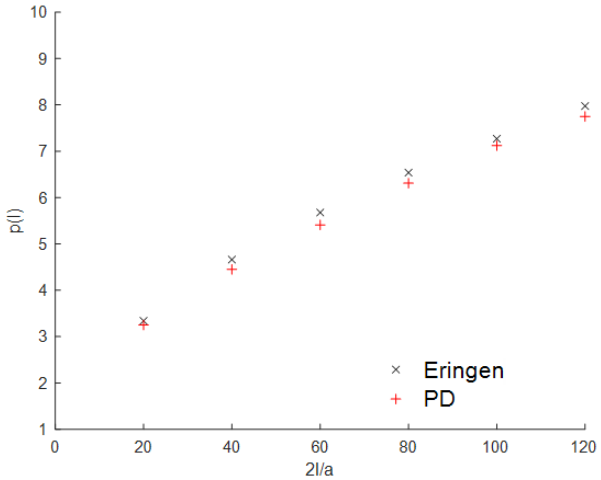

Figure 20. Comparison of the variation of the maximum stress values at the crack tip for various crack sizes between peridynamics (PD) and nonlocal elasticity (Eringen [14]) solutions.

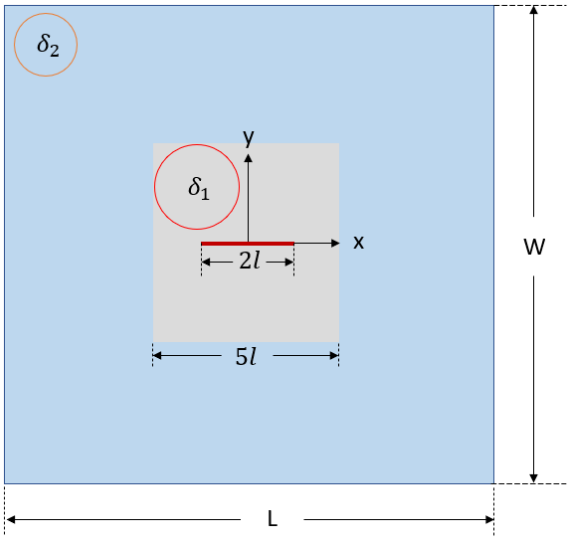

Figure 21. Dual horizon numerical domain

As shown earlier, the horizon size without damage can be obtained by using dispersion relationships. For regions away from the crack tip region, it will be more appropriate to use this horizon size. For copper, the horizon size is obtained as $\delta = 2.472\times10^{-10}\,\mathrm{m}$. Since two different horizon sizes are defined for two different parts of the solution domain, dual horizon peridynamics can be utilized as shown in Fig. 21. For a crack size of $2l = 40a$, the comparison of the vertical stress along the central x-axis for peridynamic and non-local elasticity results is presented in Fig. 22. As can be seen in this figure, a good agreement is obtained between the two solutions.

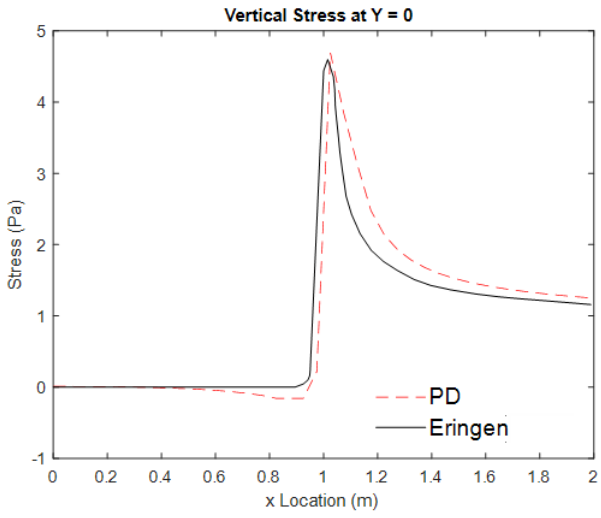

Figure 22. Comparison of the vertical stress along the central *x*-axis between peridynamics (PD) and nonlocal elasticity (Eringen [14]) solutions.

Crack Tip Damage Zone Investigation

By using the displacement field at the crack tip given in Eq. (51), the broken bonds and damaged material points are obtained for different discretization sizes and same horizon sizes as shown in Fig. 23.

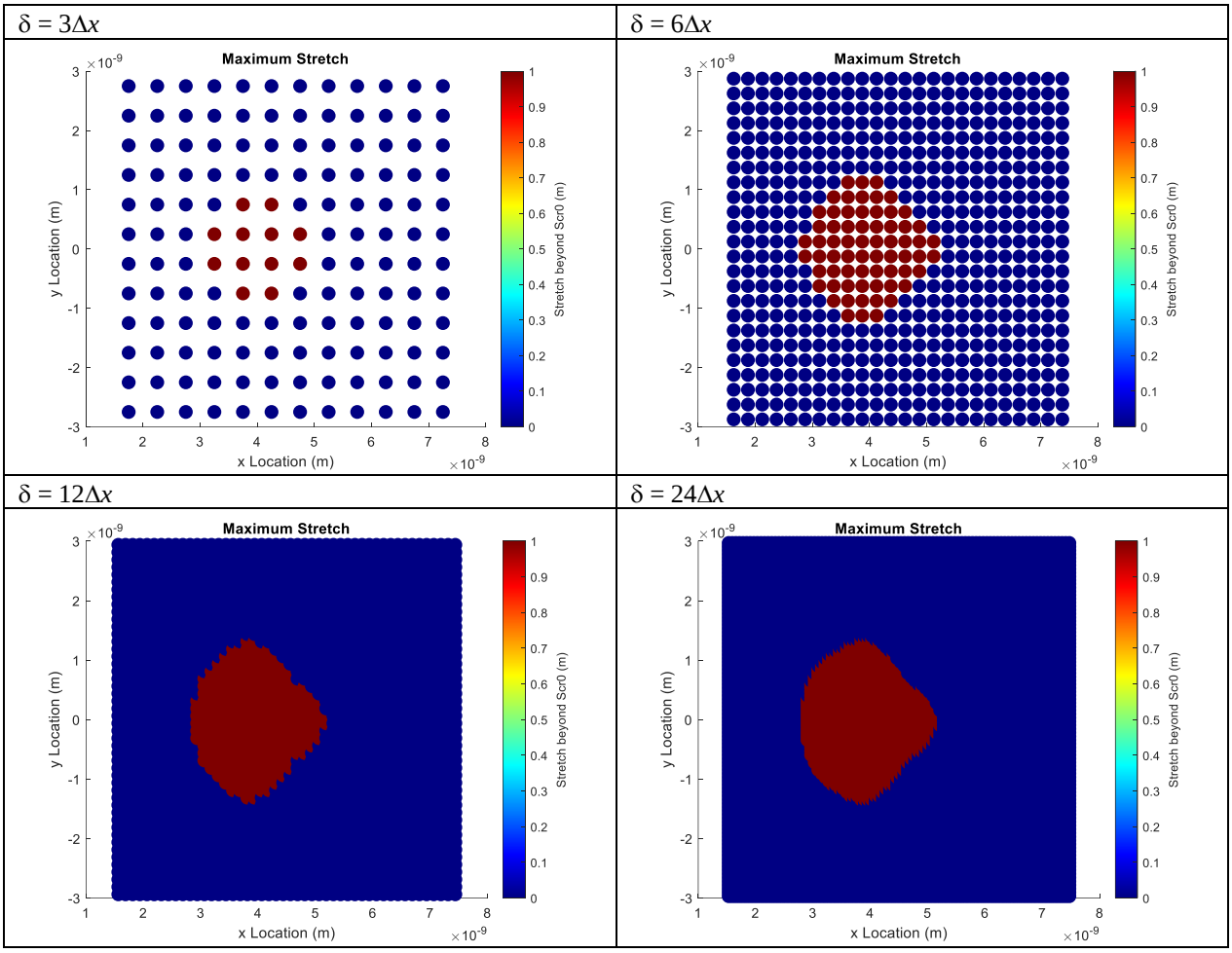

Figure 23. Damaged material points for different discretizations

Based on the damaged material points shown in Fig. 23, the damaged region has a shape given in Fig. 24.

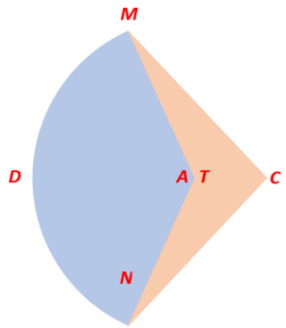

Figure 24. Shape of the damaged region around the crack tip**.**

In Fig. 24, *C* is the intersection point of line L_{MC} and line L_{NC}, T is the crack tip location, A is the centre of arc MN, D is the far endpoint of arc MN, the angle between line L_{MC} and line L_{NC} is $\angle MCN$.

To understand the meaning of the observed area, an investigation has been carried out for the horizon size when $\delta = n\Delta x$ with $n = 6, 12, 24, 32$ as shown in Fig. 25. In Fig. 25,

the ○ in 'green' is the horizon draw from *A*, the centre of arc MN;
the ○ in 'yellow' is the horizon draw from the crack tip location *T*;
the ○ in 'red' is the horizon draw from *C*, the intersection point of line L_{MC} and line L_{NC}.

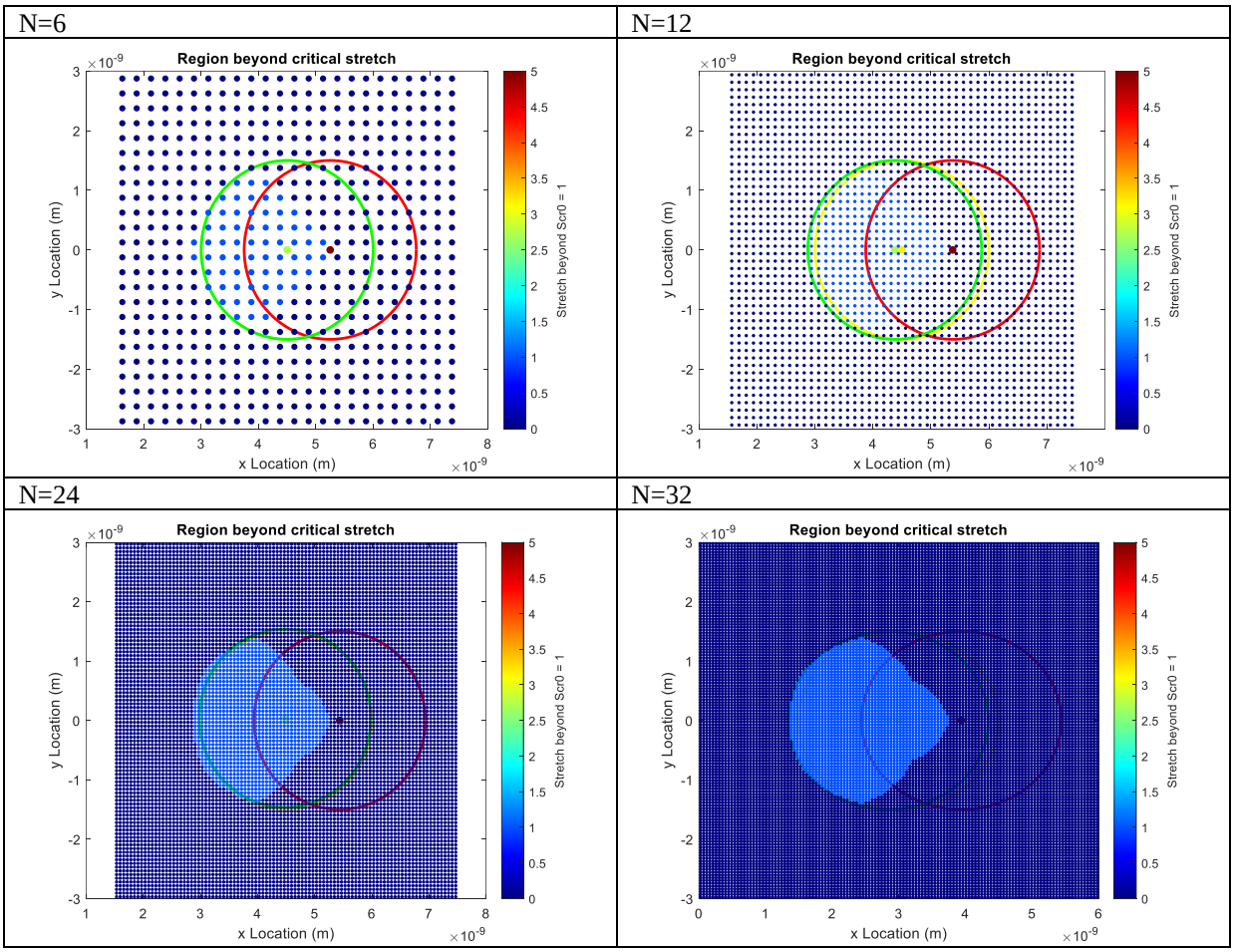

Figure 25. Investigation of damaged region for different discretizations.

Determination of Horizon Size Based on The Plasticity Field Around Crack Tip

As shown in Fig. 26, an isotropic square plate with a line crack is subjected to a tension loading along its horizontal edges. The plate has in-plane dimensions of $L = W = 1\,\text{m}$ and thickness of $h = 0.005\,\text{m}$. The crack length is specified as $2l = 0.3\,\text{m}$. Young's modulus, Poisson's ratio and density of the plate are given as $E = 200\,\text{GPa}$, $\nu = 0.3$ and $\rho = 7850\,\text{kg/m}^3$, respectively. Spacing between material points is specified as $\Delta x = 0.005\,\text{m}$. Various horizon sizes are considered as $\delta = 2\Delta x, 3\Delta x, 4\Delta x, 5\Delta x$. The plate is subjected to a tension loading of 150 MPa.

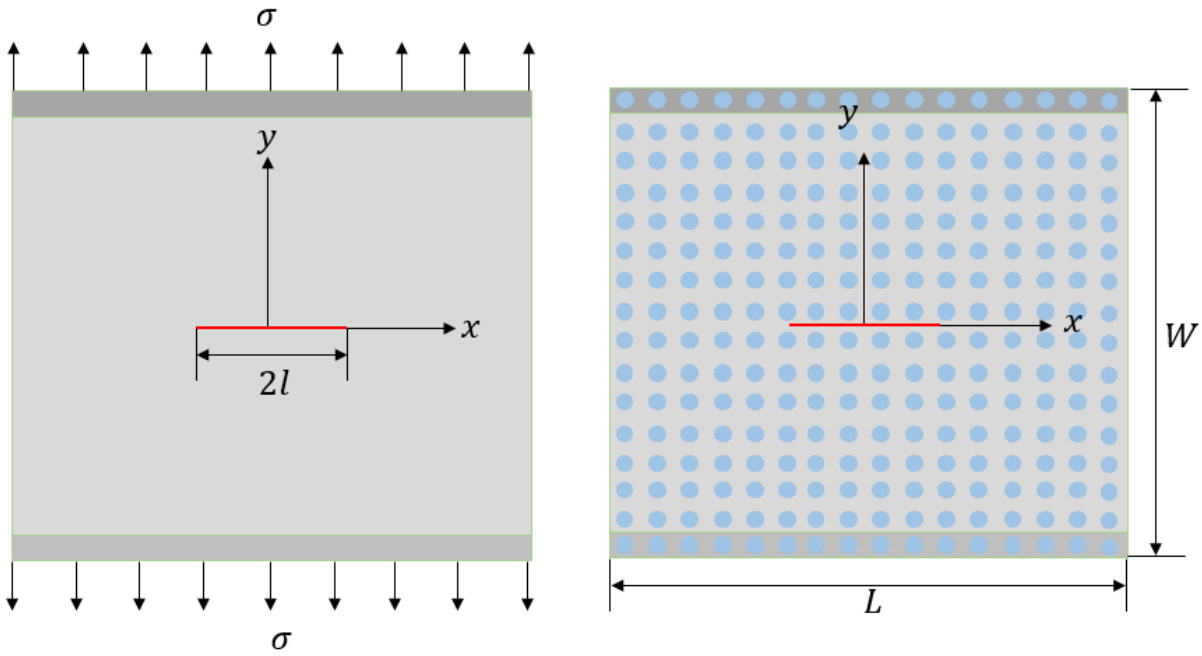

Figure 26. Plate with a central crack under tension loading

The von mises stress σ_{VM} distributions for different horizon sizes are shown in Fig. 27.

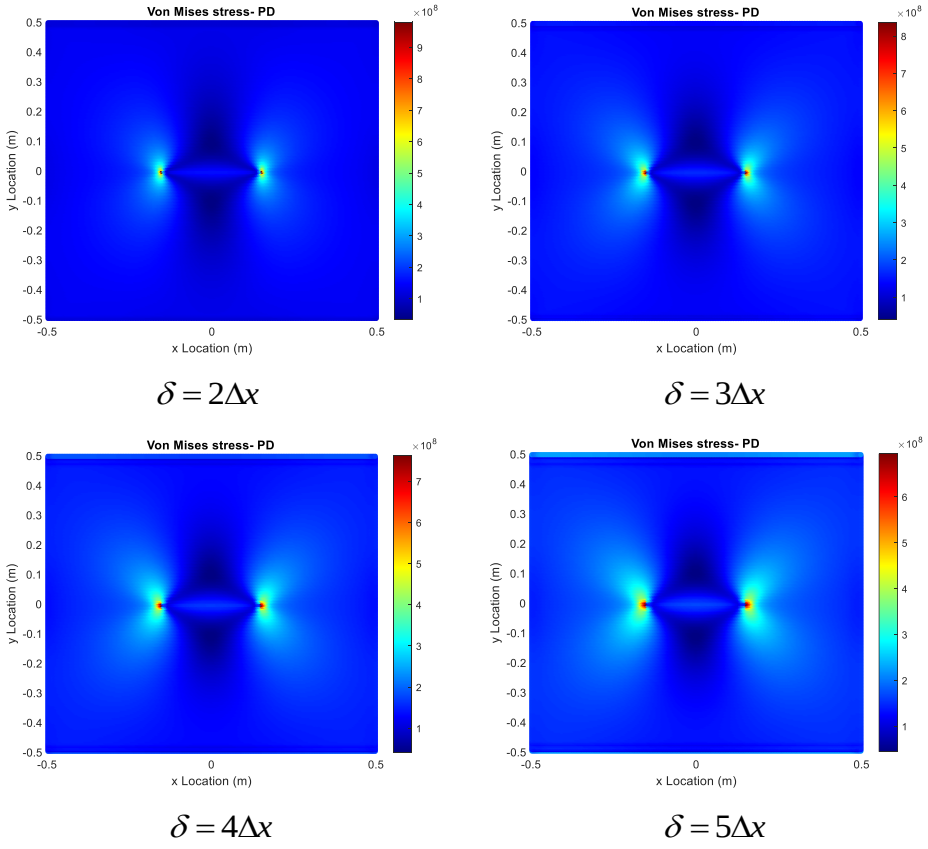

Figure 27. von Mises stress distribution for different horizon sizes.

Next, von Mises stresses are compared with yield stress value of the material, $\sigma_y = 205\text{MPa}$. The material points whose stress values are beyond the yield stress value are shown in Fig. 28. The same problem is also solved by using finite element method (FEM). By comparing peridynamic results against FEM solution, it can be concluded that the horizon size values of $\delta = 3\Delta x \text{ and } 4\Delta x$ yield the best match with FEM results.

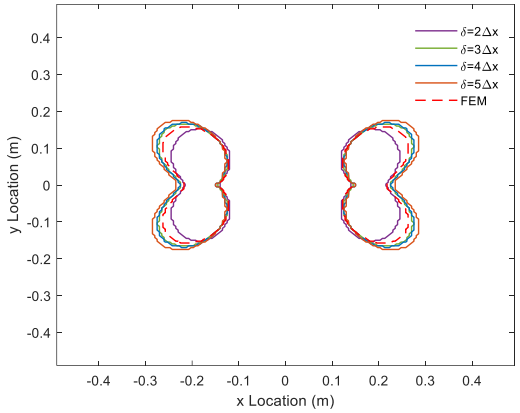

Figure 28. Material points whose stress values are beyond the yield stress value for different horizon sizes.

Multi-horizon Peridynamic Formulation

Next, a new "multi-horizon" formulation is applied for a one-dimensional bar subjected to initial displacement. As shown in Fig. 29, the bar with clamped left end and free right end is studied. The length of the bar is $L = 1\text{m}$, with cross sectional area of $A = 0.001 \times 0.001\text{m}^2$. Its elastic modulus and material density are specified as $E = 200\,\text{GPa}$ and $\rho = 7850\,\text{kg/m}^3$. The bar is discretized into one single row of material points with spacing of $\Delta x = 0.002\,\text{m}$.

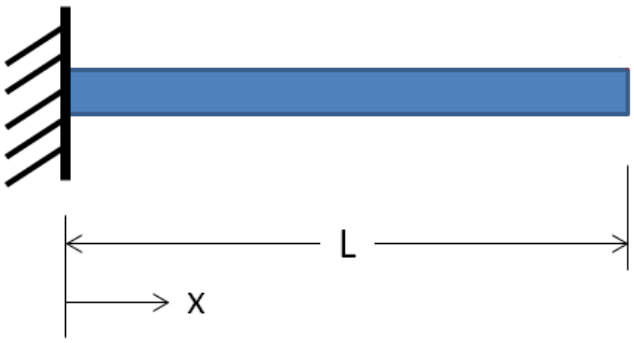

Figure 29. One-dimensional bar subjected to initial deformation.

In order to verify the accuracy and advantage of this approach, numerical results of amendatory PD (multi-horizon formulation), is compared against the classical PD solution, and analytical solution. A

material point located at x=0.998 m is monitored and the displacement variation with time is shown in Fig. 30. It can be clearly seen that three solutions agree each other well at the beginning. However, the vibration behavior of classical PD solution starts deviating as the time goes by, and amendatory PD and analytical solution agree well all through.

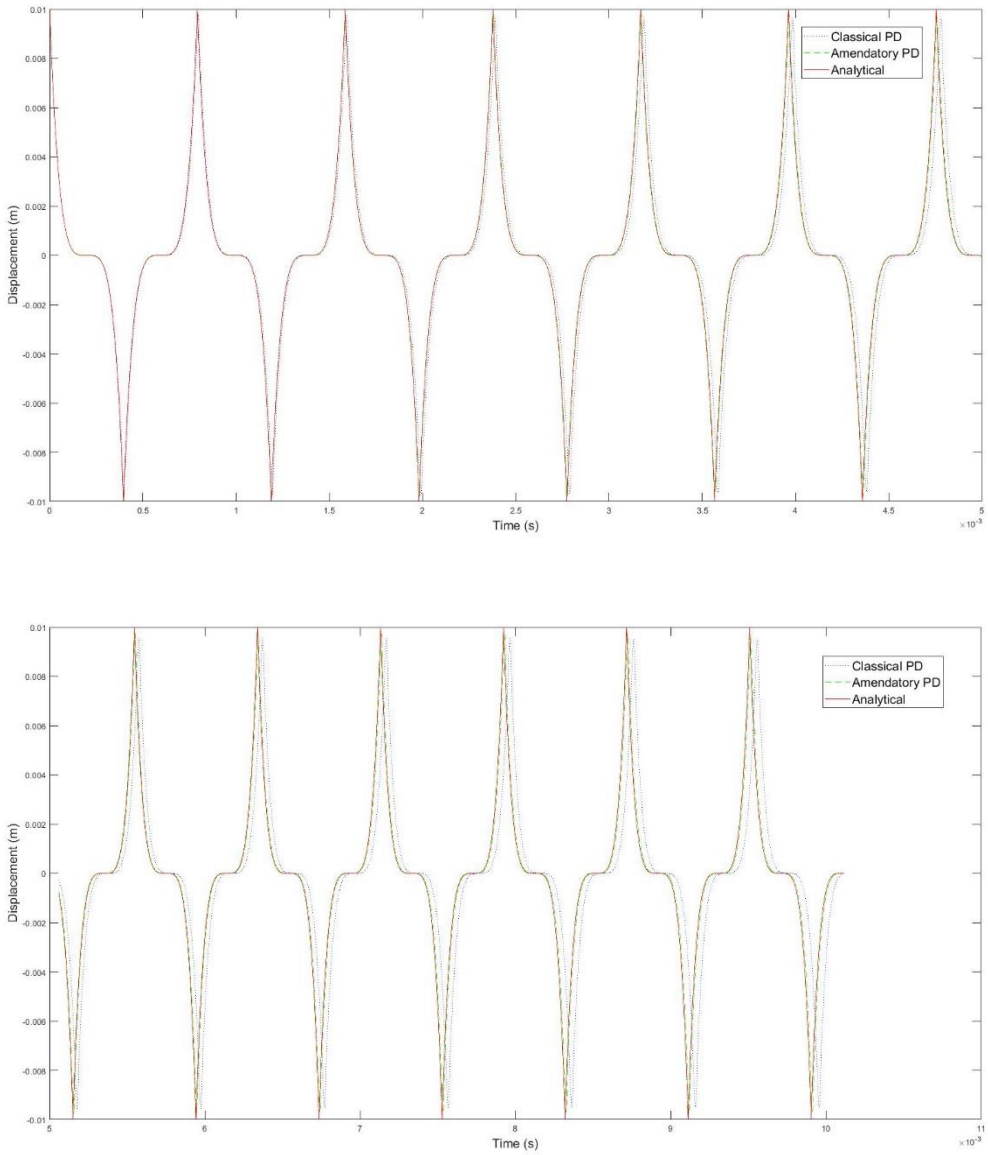

Figure 30. Variation of the displacement of the material point located at x=0.998 m.

Surface Elasticity

Peridynamics is also utilized for a surface elasticity problem to determine the effective modulus of a nanowire. In this section, the validity of the modified core-shell PD model by comparing with the MC-S discrete model for rectangular nanowires. The bulk elasticity of the rectangular nanowire is considered as $E_{bulk} = 140\ GPa$ [21] the surface layer is modelled with 4 surface materials with elastic modulus of

$$E_i = E_{bulk} e^{(\alpha(y_i - W_b))} \tag{83}$$

with $y_i = W_b + \sum_{k=1}^{i} W_{s,k}$ and $\alpha = 0.63\ (\tilde{\alpha} = 1.26)$. The thicknesses of the surface layers are taken as $W_{s,i} = 0.4\ nm,\ i = 1,2,3,4$. The rectangular nanowire is subjected to a strain of 0.01 in the longitudinal direction. The total length of the nanowire is $L = 10\ nm$.

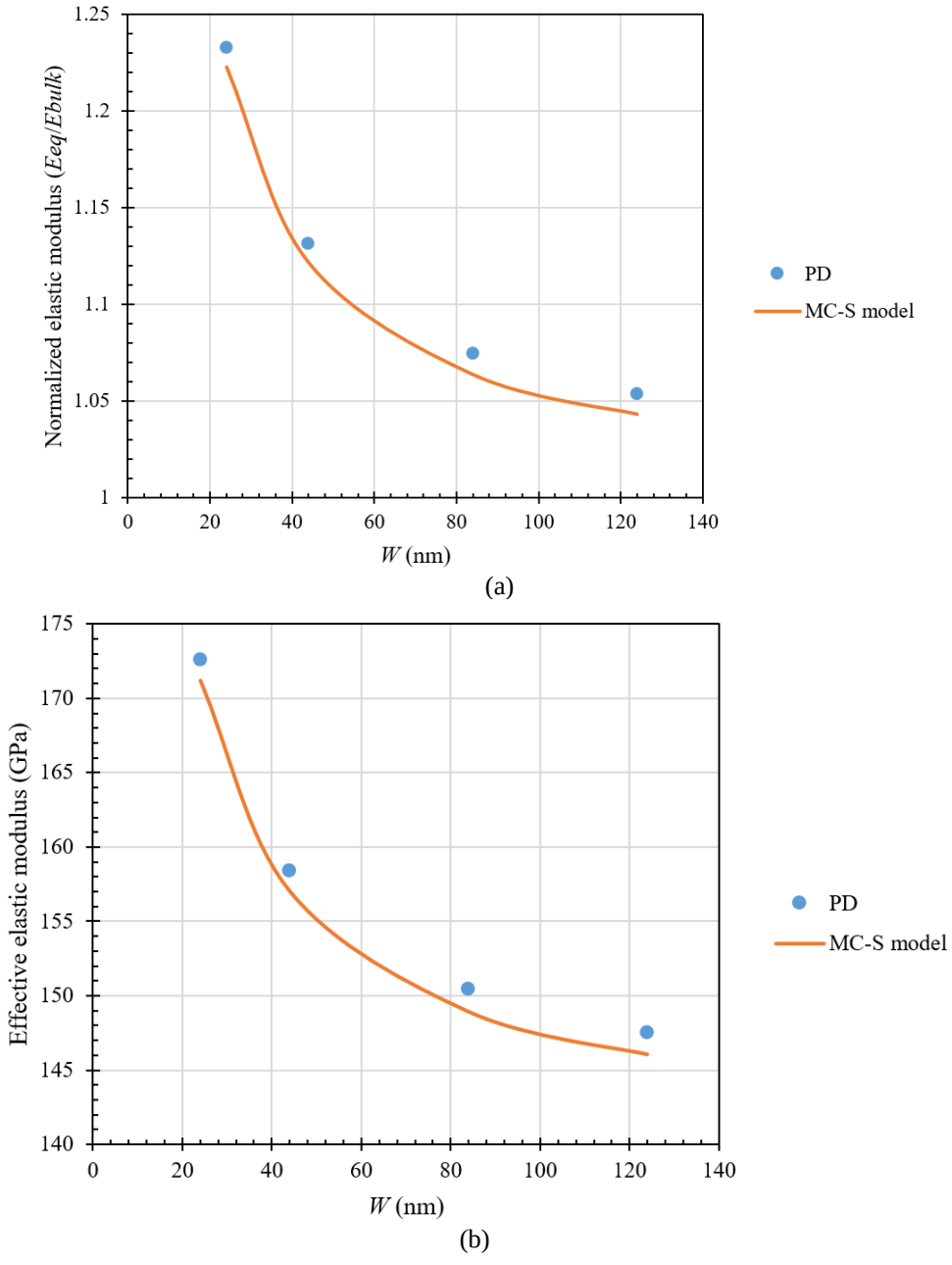

Figure 31. The size effect of the normalized elastic modulus in the longitudinal direction, E_{eq} / E_{bulk} for tension loading for [0001] oriented ZnO nanowires with $\tilde{\alpha} = 1.26$ [21], (a) Normalized elastic modulus; (b) effective elastic modulus.

As shown in Fig. 31, effective elastic modulus values obtained from peridynamics and MC-S

approach agree well with each other.

Static Condensation of the Peridynamic Heat Conduction Model

A homogeneous bar initially at zero temperature is subjected to a boundary temperature of $1^{\circ}\mathrm{C}$ at both ends as shown in Fig. 32. The bar has a length and thickness of $1\mathrm{m}$ and $0.01\mathrm{m}$, respectively. The specific heat capacity, thermal conductivity and density of the bar are specified as $C_v = 64\,\mathrm{J/kgK}$, $\kappa = 233\,\mathrm{W/mK}$ and $\rho = 260\,\mathrm{kg/m^3}$, respectively. The material of the bar is assumed to have a micro-conductivity function as $k = 2\kappa/(A\delta^2)$.

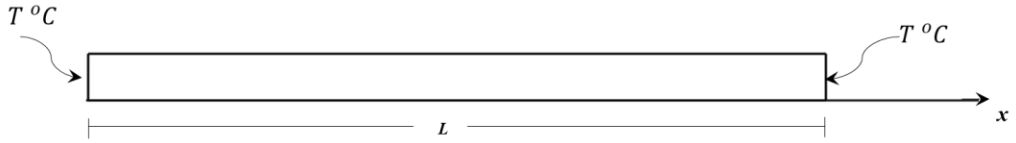

Figure 32. A homogeneous bar subjected to heat at both ends.

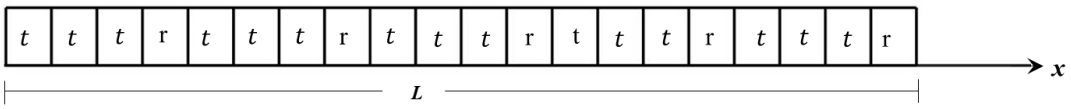

t : truncated Degree of freedom

r : retained Degree of freedom

Figure 33. A discretized bar to illustrate condensation of the micro-conductivity functions.

The bar is discretized into 100 nodes thus the spacing between nodes is $\Delta x = 0.01$. Model order reduction of the bar is achieved by retaining every fourth node of the full model as shown in Fig. 33. A time step size of $\Delta t = 10^{-2}\,\mathrm{s}$ is used and the simulation was run for 3000 time steps.

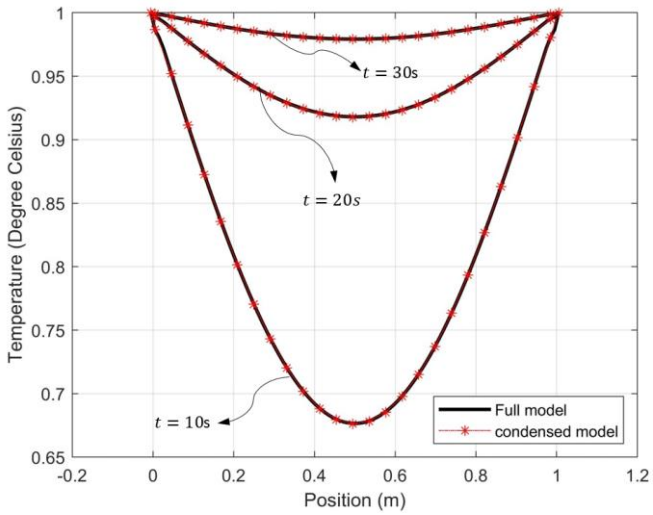

Figure 34. Temperature distribution in a homogeneous bar subjected to heat at both ends.

Temperature prediction for both full model and reduced model are presented in Fig. 34. The reported results are temperature distribution across the bar corresponding to time steps $t = 10\,\text{s}, 20\,\text{s}$ and $30\,\text{s}$. These results show a good match between the full model and reduced model thus demonstrating the capability of the model order reduction scheme in preserving the dynamics of a one-dimensional transient peridynamic heat conduction model in-spite of using fewer degrees of freedom.

The model reduction scheme also allows for adaptive implementation of the condensation algorithm so that a more detailed model can be implemented in locations where higher resolution results are needed for greater insight into the numerical predictions.

Homogenisation in non-ordinary state based peridynamics

A numerical example is presented in this section to benchmark the peridynamic correspondence homogenization theory (PDCHT). To pursue this goal, an RVE associated with a composite is assumed to consist of two constituent materials: a fiber material and a matrix. For the composite, a square RVE with a circular fiber as shown in Fig. 35 is assumed for simplicity.

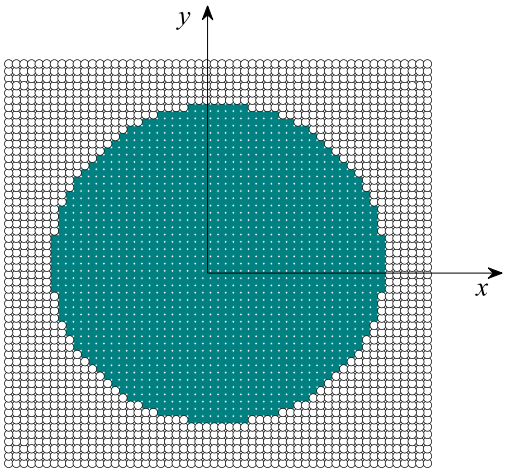

Figure 35. RVE geometry showing peridynamic discretization

This RVE is assumed to consist of boron as the fiber material and aluminum as the matrix. The properties of these constituent materials are provided in Table 1 as quoted from [22]. The RVE problem is solved for a fibre volume fraction of 0.47.

Table 1. Material properties of the constituents

	E (GPa)	ν
Matrix	379.3	0.3
Fibre	68.3	0.1

The RVE is subjected to Periodic Boundary Condition (PBC). Although computational algorithm to implement this boundary condition in the framework of finite element analysis is well established and discussed by many authors, however, implementing it in a nonlocal boundary value constraint problem such as the RVE in the PDCHT framework requires special treatment. In order to implement the PBC in the PDCHT framework, the displacement driven approach to homogenization is utilized in this study. The expression for the effective elasticity tensor can be written as

$$\mathbb{C}^*_{ijkl} = \frac{1}{V_{\Omega_s}\bar{\varepsilon}_{kl}} \int_{\Omega_s} \sigma_{ij} dV_{\Omega_s} \tag{84}$$

where σ_{ij} is the stress field and $\bar{\varepsilon}_{kl}$ is the prescribed strain tensor on the boundary volume. For a two-dimensional problem, $\mathbb{C}^*_{ijkl}$ has six components. However, owing to its symmetric property, only three components are independent. Thus, to determine the components of $\mathbb{C}^*_{ijkl}$ for a two-dimensional problem require the application of three loading conditions that result in deformation modes which render all but one of the three independent components of the strain tensor to zero. For the purpose of this implementation, these deformation modes are given as

$$\bar{\varepsilon}_{11} = \begin{bmatrix} c & 0 \\ 0 & 0 \end{bmatrix}, \bar{\varepsilon}_{22} = \begin{bmatrix} 0 & 0 \\ 0 & c \end{bmatrix}, \bar{\varepsilon}_{12} = \begin{bmatrix} 0 & 1/2c \\ 1/2c & 0 \end{bmatrix} \tag{85}$$

where c is the magnitude of the prescribed strain tensor. These strains are then used to generate displacement in the boundary volume. The determination of the effective elastic tensor proceeds under the assumption of small deformation and plane stress.

For the purpose of validating the proposed framework, results from the Peridynamic homogenization scheme is compared with results from the following sources: a finite element model of the RVE by the authors, results from an ordinary state-based homogenization scheme developed by Xia et al. [23] and prediction from references [22, 24-26] as quoted in [22].

Table 2. Effective elastic constants for boron/aluminium composite (fibre volume fraction = 0.47)

Elastic constants	PDCHT	FEM	Ref [23]	Ref [22]	Ref [24]	Ref [25]	Ref [26]
E (GPa)	140	141	150	144	156	123	135
G (GPa)	59.3	58.7	53.4	57.2	62.6	53.9	51.1
v	0.184	0.2	0.18	0.19	0.2	0.19	0.19

Table 2 shows the effective elasticity modulus, shear modulus and Poisson's ratio obtained from the PDCHT framework, alongside corresponding values from other refrences as listed above. A good agreement is observed between different approaches.

A further analysis of the results from this proposed scheme is also made by comparing the

evolution of the predicted effective material properties with those obtained from the Reuss and Voigt models. The objective is to show that the proposed methodology obeys the Reuss-Voigt bound. Based on the evaluated results, it can be concluded that the results comply with the so-called Hill-Reuss-Voigt bounds as well as agree with results from finite element simulation of the RVE. Validation of the numerical results with prediction using FEM analysis and data from the literature shows that the presented homogenization framework can provide good estimate of the effective properties of composites.

The advantage of PDCHT theory over homogenization frameworks based on the classical continuum theory, derives from the strengths of the peridynamic theory. This framework is therefore especially useful in circumstances involving evolution of the microstructure or problems in which nonlocal interaction plays important role in the overall response of the heterogenous media. Another advantage that can be leveraged with this development is that because the peridynamic correspondence model uses familiar quantities from the classical continuum theory, Once the effective material tangent is obtained, we are free to use either of peridynamic theory or the classical continuum theory to characterise the macroscopic response of the medium. Where the peridynamic theory is utilised at the macroscale, this result in a standard multigrid method we will call the PD^2 method. In the case where the classical theory is utilised, this result in what is referred to in the literature as Heterogenous Multiscale Method (HMM) [27]. In this case, numerical schemes such as the finite element method or the finite difference method can be utilised to solve the macro model.

References

[1] Silling, S.A., 2000. Reformulation of elasticity theory for discontinuities and long-range forces. *Journal of the Mechanics and Physics of Solids*, *48*(1), pp.175-209.

[2] Madenci, E. and Oterkus, E., 2014. *Peridynamic theory and its applications*. New York: Springer.

[3] Dugdale, D.S., 1960. Yielding of steel sheets containing slits. *Journal of the Mechanics and Physics of Solids*, *8*(2), pp.100-104.3

[4] Madenci, E. and Oterkus, S., 2016. Ordinary state-based peridynamics for plastic deformation according to von Mises yield criteria with isotropic hardening. *Journal of the Mechanics and Phy sics of Solids*, *86*, pp.192-219

[5] Gu, X., Madenci, E. and Zhang, Q., 2018. Revisit of non-ordinary state-based peridynamics. *Engineering Fracture Mechanics*, 190, pp.31-52.

[6] Silling, S.A., 2017. Stability of peridynamic correspondence material models and their particle dis cretizations. *Computer Methods in Applied Mechanics and Engineering*, *322*, pp.42-57.

[7] Silling, S.A. and Askari, E., 2005. A meshfree method based on the peridynamic model of solid mechanics. *Computers & structures*, *83*(17-18), pp.1526-1535.

[8] Wang, B., Oterkus, S. and Oterkus, E., 2020, "Determination of horizon size in state-based peridynamics," *Continuum Mechanics and Thermodynamics*, available online.

[9] Wang, B., Oterkus, S. and Oterkus, E., 2020, "Derivation of Dual Horizon State-based Peridynamics Formulation Based on Euler-Lagrange Equation," *Continuum Mechanics and Thermodynamics*, available online.

[10] Wang, B., Oterkus, S. and Oterkus, E., 2021, "Thermal Diffusion Analysis by Using Dual Horizon Peridynamics," *Journal of Thermal Stresses*, Vol. 44(1), pp. 51-74.
[11] Oterkus, S., Wang, B. and Oterkus. E., 2020, "Effect of Horizon Shape in Peridynamics," *Structural Integrity Procedia*, Vol. 28, pp. 418-429.
[12] Wang, B., Oterkus, S. and Oterkus, E., 2020, "Closed-form Dispersion Relationships in Bond-based Peridynamics," *Structural Integrity Procedia*, Vol. 28, pp. 482-490.
[13] Wang, B., Oterkus, S. and Oterkus, E., "Comparison of Peridynamics and Lattice Dynamics Wave Dispersion Relationships," submitted to *Journal of Peridynamics and Nonlocal Modeling*.
[14] Eringen, A.C., Speziale, C.G. and Kim, B.S., 1977. Crack-tip problem in non-local elasticity. *Journal of the Mechanics and Physics of Solids*, *25*(5), pp.339-355.
[15] Elliott, H.A., 1947. An analysis of the conditions for rupture due to Griffith cracks. *Proceedings of the Physical Society (1926-1948)*, *59*(2), p.208.
[16] Gohar, A.Y., 1979. *Microscopic Fracture Study in the Two-Dimensional Triangular Lattice* (Doctoral dissertation, City University of New York).
[17] Yao H, Yun G, Bai N, Li J. Surface elasticity effect on the size-dependent elastic property o f nanowires. Journal of Applied Physics. 2012 Apr 15;111(8):083506.
[18] Oterkus, S. and Oterkus, E., "Peridynamic Surface Elasticity Formulation Based on Modified Core-shell Model," submitted to *Journal of Peridynamics and Nonlocal Modeling*
[19] Galadima, Y. K., Xia, W., Oterkus, E., and Oterkus, S., "A Computational Homogenization Framework for Non-ordinary State-based Peridynamics," submitted to *Engineering with Computers*.
[20] Galadima, Y. K., Oterkus, E., and Oterkus, S., "Static Condensation of Peridynamic Heat Conduction Model," submitted to *Mathematics and Mechanics of Solids*.
[21] Periodictable.com. 2020. *Young Modulus For All The Elements In The Periodic Table*. [online] Available at: <https://periodictable.com/Properties/A/YoungModulus.v.html> [Accessed 31 May 2020].
[22] Sun, C.T. and Vaidya, R.S., 1996. Prediction of composite properties from a representative volume element. *Composites science and Technology*, *56*(2), pp.171-179.
[23] Xia, W., Oterkus, E. and Oterkus, S., 2021. Ordinary state-based peridynamic homogenization of periodic micro-structured materials. *Theoretical and Applied Fracture Mechanics*, *113*, p.102960.
[24] Chamis, C.C., 1983. Simplified composite micromechanics equations for hygral, thermal and mechanical properties.
[25] Whitney, J.M. and Riley, M.B., 1966. Elastic properties of fiber reinforced composite materials. *Aiaa Journal*, *4*(9), pp.1537-1542.
[26] Sun, C.T. and Chen, J.L., 1991. A micromechanical model for plastic behavior of fibrous composites. *Composites Science and Technology*, *40*(2), pp.115-129.
[27] Vanden-Eijnden, E., 2007. Heterogeneous multiscale methods: a review. *Communications in Computational Physics2 (3)*, pp.367-450.

List of Publications and Significant Collaborations that resulted from your AOARD supported project:

a) papers published in peer-reviewed journals,

Wang, B., Oterkus, S. and Oterkus, E., 2021, "Thermal Diffusion Analysis by Using Dual Horizon Peridynamics," *Journal of Thermal Stresses*, Vol. 44(1), pp. 51-74.

Wang, B., Oterkus, S. and Oterkus, E., 2020, "Closed-form Dispersion Relationships in Bond-based Peridynamics," *Structural Integrity Procedia*, Vol. 28, pp. 482-490.

Oterkus, S., Wang, B. and Oterkus. E., 2020, "Effect of Horizon Shape in Peridynamics," *Structural Integrity Procedia*, Vol. 28, pp. 418-429.

Wang, B., Oterkus, S. and Oterkus, E., 2020, "Derivation of Dual Horizon State-based Peridynamics Formulation Based on Euler-Lagrange Equation," *Continuum Mechanics and Thermodynamics*, available online.

Wang, B., Oterkus, S. and Oterkus, E., 2020, "Determination of horizon size in state-based peridynamics," *Continuum Mechanics and Thermodynamics*, available online.

b) papers published in peer-reviewed conference proceedings,

N/A

c) papers published in non-peer-reviewed journals and conference proceedings,

N/A

d) conference presentations without papers,

Nguyen, C. T., Oterkus, S. and Oterkus, E., 2021, "A Physics-guided Machine Learning Model Based on Peridynamics" ASME 2021 International Mechanical Engineering Congress & Exposition, 1-5 November 2021, Virtual Conference, Online.

Oterkus S. and Oterkus, E., 2021, "Peridynamic Surface Elasticity Formulation Based on Modified Core-Shell Model," 2nd International Workshop on Plasticity, Damage and Fracture of Engineering Materials, 18-20 August 2021, Virtual Conference, Online.

Wang, B., Oterkus S. and Oterkus, E., 2021, "Comparison of Peridynamics and Lattice Dynamics Wave Dispersion Relationships," 2nd International Workshop on Plasticity, Damage and Fracture of Engineering Materials, 18-20 August 2021, Virtual Conference, Online.

Oterkus, S., Wang, B. and Oterkus, E., 2021, "Dual Horizon Peridynamic Formulation for Thermal Diffusion Analysis," 16th U.S. National Congress on Computational Mechanics (USNCCM), 25-29 July 2021, Virtual Conference, Online.

Wang, B., Oterkus, S. and Oterkus, E., 2020, "Wave Dispersion in Peridynamics" ASME 2020 International Mechanical Engineering Congress & Exposition, 16-19 November 2020, Virtual Conference, Online.

Wang, B., Oterkus, S. and Oterkus, E., 2020, "Peridynamic Modeling with Non-uniform Discretisation and Variable Horizon" ASME 2020 International Mechanical Engineering Congress & Exposition, 16-19 November 2020, Virtual Conference, Online.

Oterkus, E., Wang, B., and Oterkus, S., 2020, "Utilisation of Euler-Lagrange Equation to Derive Dual-Horizon Peridynamic Equations," 3rd Annual Meeting of the SIAM Texas-Louisiana Section, 16-18 October 2020, College Station, TX, USA.

Oterkus, S., Wang, B. and Oterkus, E., 2020, "Effect of Horizon Shape in Peridynamics," 1st Virtual European Conference on Fracture (VECF1), Online, June 29 – July 1, 2020.

Wang, B., Oterkus, S., and Oterkus, E., 2020, "Closed-Form Dispersion Relationships in Bond-Based Peridynamics," 1st Virtual European Conference on Fracture (VECF1), Online, June 29 – July 1, 2020.

e) manuscripts submitted but not yet published,

Galadima, Y. K., Xia, W., Oterkus, E., and Oterkus, S., "A Computational Homogenization Framework for Non-ordinary State-based Peridynamics," submitted to *Engineering with Computers*.

Galadima, Y. K., Oterkus, E., and Oterkus, S., "Static Condensation of Peridynamic Heat Conduction Model," submitted to *Mathematics and Mechanics of Solids*.

Wang, B., Oterkus, S. and Oterkus, E., "Comparison of Peridynamics and Lattice Dynamics Wave Dispersion Relationships," submitted to *Journal of Peridynamics and Nonlocal Modeling*.
Oterkus, S. and Oterkus, E., "Peridynamic Surface Elasticity Formulation Based on Modified Core-shell Model," submitted to *Journal of Peridynamics and Nonlocal Modeling*

and

f) provide a list any interactions with industry or with Air Force Research Laboratory scientists or significant collaborations that resulted from this work.

Attachments: Publications a), b), c) and d) listed above if possible.

DD882: As a separate document, please complete and sign the inventions disclosure form.

Important Note: If the work has been adequately described in refereed publications, submit an abstract as described above and refer the reader to your above List of Publications for details. If a full report needs to be written, then submission of a final report that is very similar to a full length journal article will be sufficient in most cases. This document may be as long or as short as needed to give a fair account of the work performed during the period of performance. There will be variations depending on the scope of the work. As such, there is no length or formatting constraints for the final report. Keep in mind the amount of funding you received relative to the amount of effort you put into the report. For example, do not submit a $300k report for $50k worth of funding; likewise, do not submit a $50k report for $300k worth of funding. Include as many charts and figures as required to explain the work.